Bouchez, J., von Blanckenburg, F., Schuessler, J. A. (2013): Modeling novel stable isotope ratios in the weathering zone. - American Journal of Science, 313, 4, 267-308

DOI: 10.2475/04.2013.01

[American Journal of Science, Vol. 313, April, 2013, P. 267–308, DOI 10.2475/04.2013.01]

American Journal of Science

APRIL 2013

MODELING NOVEL STABLE ISOTOPE RATIOS IN THE WEATHERING ZONE

JULIEN BOUCHEZ, FRIEDHELM VON BLANCKENBURG, and JAN A. SCHUESSLER

GFZ German Research Centre for Geosciences, Helmholtz Centre Potsdam, Telegrafenberg, 14473 Potsdam, Germany; bouchez@gfz-potsdam.de

ABSTRACT. When rock is converted to weathering products, the involved processes can be fingerprinted using the stable isotope ratios of metals (for example Li, Mg, Ca, Fe, Sr) and metalloids (B, Si). Here we construct a framework for interpreting these "novel" stable isotope ratios quantitatively in the compartments of the weathering zone in a geomorphic context. The approach is applicable to any novel stable isotope system and is based on a simple steady-state mass balance model that represents the weathering zone from the scale of a soil column to that of entire continents. Our model is based on the assumption that the two main processes associated with isotope fractionation are formation of secondary precipitates such as clays, and uptake of nutrients by plants.

The model results show that the isotope composition of a given element in the weathering zone compartments depends on (1) the ratio between the release flux to water through primary mineral dissolution and the erosion flux of isotopically fractionated solid material, consisting of secondary precipitates and organic matter; (2) the isotope fractionation factors associated with secondary mineral precipitation and uptake by plants. A relationship is established between isotope ratios, isotope fractionation factors, and indexes for chemical weathering [such as chemical depletion fractions (CDF) and elemental mass transfer coefficients (τ)] derived from simple elemental concentration measurements. From this relationship, isotope fractionation factors can be calibrated from chemical and isotope data measured on field material. Furthermore, we show how the ratio of solid export to dissolved export of a given element from the weathering system can be estimated from the comparison of the isotope composition between bedrock, water, and sediment. This calculation can be applied to samples from soils, from rivers, and from the sedimentary record, and does not require knowing the isotope fractionation factors involved in the reactions. Finally, we apply the model to the oceanic Li isotope record reconstructed from marine carbonate sediments in order to discuss changes in global geomorphic regimes through the Cenozoic.

Key words: Novel stable isotopes, box-model, weathering regime, Critical Zone, river geochemistry, isotope fractionation factors; soils

INTRODUCTION

The weathering zone is the thin layer covering the Earth's continental surface. In this layer chemical elements are released from rocks by exposure to water and atmospheric gases. The products of this weathering process, dissolved elements and mobile soil particles, are drained or eroded away and transported by rivers. Weathering constitutes the main port of entry of metal and metalloid nutrients (for example Mg, Si, K, Ca, Fe, Zn) into ecosystems. Over longer time scales, these processes act as a major geological pump of atmospheric CO_2 through silicate weathering and carbon uptake by biota (Goudie and Viles, 2012). The overarching goals of research dealing

with the weathering zone are therefore to (1) identify the processes at play in the weathering zone, (2) quantify the fluxes of matter resulting from these processes, (3) identify the controls over these processes, (4) envisage and assess the potential feedback mechanisms between these processes, as well as their relation to forcings that are external to the weathering zone itself, such as climate or tectonics.

The weathering zone can be divided into several conceptual compartments, such as unweathered substrate, bulk saprolite, bulk soil, plants, plant litter, secondary precipitates like clays or Fe-Al-Mn oxy-hydroxides, soil water and river water, and river sediment. The chemical composition of these compartments is controlled by the partitioning of elements during various weathering reactions. When combined with estimates of the flux of material from the weathering zone through, for example, measurement of river loads or of cosmogenic nuclides, the rates can be quantified and the forces driving the supply of material into and from the weathering zone can be identified (Anderson and others, 2007; Maher, 2010; Brantley and Lebedeva, 2011). In particular, the relationships between chemical weathering and physical erosion have been mapped out in detail (for example Gaillardet and others, 1999; Dupre and others, 2003; Riebe and others, 2004; West and others, 2005; Dixon and others, 2009; Dixon and von Blanckenburg, 2012).

However, element concentrations per se are imperfect tracers of physico-chemical processes in the weathering zone. In contrast, the mass-dependent fractionation of the stable isotopes of metals (for example Li, Ca, Mg, Fe, Cu, Zn, Sr) and metalloids (B, Si) produces powerful fingerprints of the processes transferring matter within, to and from the weathering zone. These fingerprints rely on the fact that each physico-chemical process is associated with a characteristic shift in the isotope ratios of the participating elements. The metals and metalloid elements, of which isotope compositions have been measured with sufficient accuracy and precision for roughly fifteen years (Halliday and others, 1998), are central players in the processes occurring in the weathering zone.

A series of recent studies based on these "novel" stable isotope systems have mapped out the isotopic composition of the different compartments in the weathering zone. The isotope systems of which the behavior in soils is best characterized are $^{7}Li/^{6}Li$ (Pistiner and Henderson, 2003; Huh and others, 2004; Kisakürek and others, 2004; Rudnick and others, 2004; Lemarchand and others, 2010; Teng and others, 2010; Pogge von Strandmann and others, 2012), $^{11}B/^{10}B$ (Spivack and others, 1987; Cividini and others, 2010; Lemarchand and others, 2012), $^{26}Mg/^{24}Mg$ (Tipper and others, 2010a; Teng and others, 2010; Bolou-Bi and others, 2012; Pogge von Strandmann and others, 2012; Opfergelt and others, 2012a; Huang and others, 2012), $^{30}Si/^{28}Si$ (Ziegler and others, 2005a, 2005b; Opfergelt and others, 2009, 2010, 2011, 2012b; Bern and others, 2010; Cornelis and others, 2010, 2011; Steinhoefel and others, 2011; Pogge von Strandmann and others, 2012), $^{44}Ca/^{42/40}Ca$ (Wiegand and others, 2005; Ewing and others, 2008; Cenki-Tok and others, 2009; Holmden and Bélanger, 2010; Hindshaw and others, 2011), $^{56}Fe/^{54}Fe$ (Fantle and DePaolo, 2004; Emmanuel and others, 2005; Thompson and others, 2007; Wiederhold and others, 2007a, 2007b; Poitrasson and others, 2008; Kiczka and others, 2011; Yesavage and others, 2012), and $^{88}Sr/^{86}Sr$ (de Souza and others, 2010). Several studies have explored these isotope systems at the scale of rivers (Huh and others, 1998, 2001; De La Rocha and others, 2000; Ding and others, 2004, 2011; Kisakürek and others, 2005; Bergquist and Boyle, 2006; Ingri and others, 2006; Georg and others, 2006, 2007, 2009a; Pogge von Strandmann and others, 2006, 2008, 2010; Lemarchand and Gaillardet, 2006; Tipper and others, 2006a, 2006b, 2008a, 2012a, 2012b; Brenot and others, 2008; Chetelat and others, 2009; Engström and others, 2010; Cardinal and others, 2010; Wimpenny and others, 2010a, 2011; Millot and others, 2010; Louvat and others, 2011; Hughes and

others, 2011; Ilina and others, 2013), aquifers (Jacobson and Holmden, 2008; Georg and others, 2009a, 2009b; Jacobson and others, 2010; Négrel and others, 2010, 2012), and oceans (Zhu and McDougall, 1998; Lemarchand and others, 2000, 2002; Schmitt and others, 2003; Wischmeyer and others, 2003; De La Rocha and Bickle, 2005; de Villiers and others, 2005; Tipper and others, 2006a, 2006b, 2010b).

In spite of the significant progress made in these studies, we still lack the ability to pinpoint the important processes resulting in isotope shifts due to general scarcity of the relevant isotope fractionation factors associated with the wide range of weathering reactions. These isotope fractionation factors are the sole parameters that link a shift in an isotope ratio to a specific process. A recent study by DePaolo (2011) emphasized the relative contribution of both thermodynamic equilibrium and kinetic effects to rate-dependent isotope fractionation factors. This rate dependence might render the application of equilibrium isotope fractionation factors determined by laboratory experiments (for example Welch and others, 2003; Vigier and others, 2008; Kiczka and others, 2010; Pearce and others, 2012) or from first principles calculations (for example Schauble and others, 2009) to natural settings less straightforward, and suggests that calibrating isotope fractionation factors from well characterized field sites does provide useful information to bridge the gap between experimental and theoretical studies. However, even if this strategy is pursued, a framework enabling the interpretation of novel isotope ratios within a geomorphic context is required; yet this framework is not in place. Such a framework shall allow us to attribute measured isotope compositions of natural samples to distinct chemical and physical processes at play in the weathering zone. This approach shall also be suited to calibrate isotope fractionation factors from field measurements provided that the fluxes are known and processes have already been identified by other means. Furthermore, a related practical question is the design of a suitable strategy for sampling the weathering zone: which compartments yield the strongest isotopic signature for a given isotope fractionation factor and as a function of the chemical behavior of the element under consideration? Finally, it should be possible to reconstruct past weathering processes from the sedimentary record in which such isotope ratios are preserved (De La Rocha and others, 1998; De La Rocha and DePaolo, 2000; Fantle and DePaolo, 2005; Hathorne and others, 2006; Sime and others, 2007; Paris and others, 2010; Fantle, 2010; Misra and Froelich, 2012).

In this paper, we construct this framework using a conceptual and mathematical model. The model is solely based on steady-state elemental and isotopic mass balance equations amongst the different compartments of the weathering zone. Previous mass balance models have already been designed to model isotope fractionation in the weathering zone for individual elements (for example Emmanuel and others, 2005; Thompson and others, 2007; Ewing and others, 2008; Cenki-Tok and others, 2009; Cividini and others, 2010; Lemarchand and others, 2010; Holmden and Bélanger, 2010; Bolou-Bi and others, 2012). Here, we take the modeling approach further by designing a generic model that is potentially applicable to any element affected by stable isotope fractionation. With this model we (1) link novel stable isotope ratios with weathering processes via element fluxes; (2) present an approach that is applicable to spatial scales that range from the soil column to large rivers or even entire continents; (3) enable calibrating isotope fractionation factors based on isotope measurements of field materials; (4) discuss the possibility to determine past denudation rates or geomorphic regimes when metal or metalloid elements are preserved in the sedimentary record.

MODEL DESCRIPTION

In this section, we first describe our conceptual model for the weathering zone, and then establish a series of elemental and isotope steady-state mass balance equa-

TABLE 1

Summary of symbols

	Total mass fluxes (for example in kg m^{-2} yr^{-1})
RP	Regolith production [$RP = D$ at steady-state]
E	Erosion
W	Weathering
D	Denudation [$D = E + W$ at steady-state]
	Dimensional elemental fluxes F^X (for example in mol_X m^{-2} yr^{-1})
S^X_{rock}	Dissolution ("solubilization") of X from primary minerals at the weathering front
RP^X_{prim}	Transfer of X in primary minerals from bedrock to regolith at the weathering front
W^X	Dissolved export of X ("weathering")
E^X	Particulate export of X ("erosion") [$E^X = E^X_{prim} + E^X_{sec} + E^X_{org}$ by definition]
U^X	Uptake of X by plants [$U^X = L^X$ at steady-state]
L^X	Flux of X from plants to soil through litter fall
P^X	Incorporation of X into secondary weathering products (including adsorption)
S^X_{prim}	Dissolution of X ("solubilization") from primary minerals in the regolith
E^X_{prim}	Erosion of X contained in primary minerals [$E^X_{prim} = RP^X_{prim} - S^X_{prim}$ at steady-state]
S^X_{sec}	Dissolution of X ("solubilization") from secondary weathering products in the regolith
E^X_{sec}	Erosion of X contained in secondary weathering products [$E^X_{sec} = P^X - S^X_{sec}$ at steady-state]
S^X_{org}	Dissolution of X ("solubilization") from organic matter in the regolith
E^X_{org}	Erosion of X contained in organic matter [$E^X_{org} = L^X - S^X_{org}$ at steady-state]
	Non-dimensional elemental fluxes f^X (fractions of $S^X{}_{rock} + RP^X{}_{prim} = D \cdot [X]_{rock}$)
s^X_{rock}	Dissolution ("solubilization") of X from primary minerals at the weathering front [$s^X_{rock} < 1$]
rp^X_{prim}	Transfer of X in primary minerals from bedrock to regolith at the weathering front [$rp^X_{prim} < 1$]
w^X	Dissolved export of X ("weathering") [$w^X < 1$]
e^X	Particulate export of X ("erosion") [$e^X < 1$ and $e^X = e^X_{prim} + e^X_{org} + e^X_{sec}$ by definition]
u^X	Uptake of X by plants [indicates the biological recycling rate]
l^X	Flux of X from plants to soil through litter fall [indicates the biological recycling rate]
p^X	Incorporation of X into secondary weathering products (including adsorption) [indicates the "inorganic" recycling rate]
s^X_{prim}	Dissolution of X ("solubilization") from primary minerals in the regolith
e^X_{prim}	Erosion of X contained in primary minerals [$e^X_{prim} < e^X < 1$]
s^X_{sec}	Dissolution of X ("solubilization") from secondary weathering products in the regolith
e^X_{sec}	Erosion of X contained in secondary weathering products [$e^X_{sec} < e^X < 1$]
s^X_{org}	Dissolution of X ("solubilization") from organic matter in the regolith
e^X_{org}	Erosion of X contained in organic matter [$e^X_{org} < e^X < 1$]

TABLE 1
(continued)

	Isotope composition (in ‰)
δ^X_{rock}	Isotope composition of X in bedrock
δ^X_{prim}	Isotope composition of X in regolith primary minerals
δ^X_{sec}	Isotope composition of X in secondary weathering products
δ^X_{org}	Isotope composition of X in regolith organic matter
δ^X_{veg}	Isotope composition of X in vegetation
δ^X_{sed}	Isotope composition of X in bulk top soil or rover sediment
δ^X_{diss}	Isotope composition of X in soil- or river water
	Isotope fractionation factor (in ‰)
Δ^X_{prec}	Isotope fractionation factor associated with precipitation of secondary weathering products (including adsorption)
Δ^X_{upt}	Isotope fractionation factor associated with uptake by plants
$\overline{\Delta}^X$	"Lumped" isotope fractionation factor [includes precipitation and uptake by plants]
	Concentrations (for example in $mol_X\,kg^{-1}$)
$[X]_{rock}$	Concentration in of X in bulk bedrock
$[X]_{prim}$	Concentration of primary mineral-bound X in the regolith
$[X]_{sec}$	Concentration of secondary weathering products-bound X in the regolith
$[X]_{org}$	Concentration of organic matter-bound X in the regolith
	Weathering indexes (dimensionless)
τ^X	Mass transfer coefficient of X
τ^X_{prim}	Mass transfer coefficient of primary mineral-bound X
CDF	Chemical depletion fraction

tions that are used to predict the isotope composition of the weathering zone compartments. Symbols are listed in table 1. The assumptions the model is based on are later discussed in detail.

The Compartments

Five compartments represent the fundamental components of our model weathering zone, regardless of the considered geographical area or geomorphological setting. We lump saprolite and soil under the term regolith, defined as the mantle of unconsolidated and weathered solid material found above unweathered bedrock (Brantley and others, 2011). We divide the regolith into three conceptual compartments based on their mineralogical and structural composition, and on their genetic processes (fig. 1): (1) unweathered, primary minerals; (2) secondary, solid weathering products comprising elements adsorbed onto mineral surfaces, precipitates of amorphous alumino-silicates, Al-Fe oxi-hydroxides, clay minerals as well as pedogenic carbonates; (3) solid organic material derived from litter fall or dead roots. The water percolating through the regolith and reacting with solid is termed here the “soil water” compartment (fig. 1), and includes both the dissolved organic and inorganic chemical

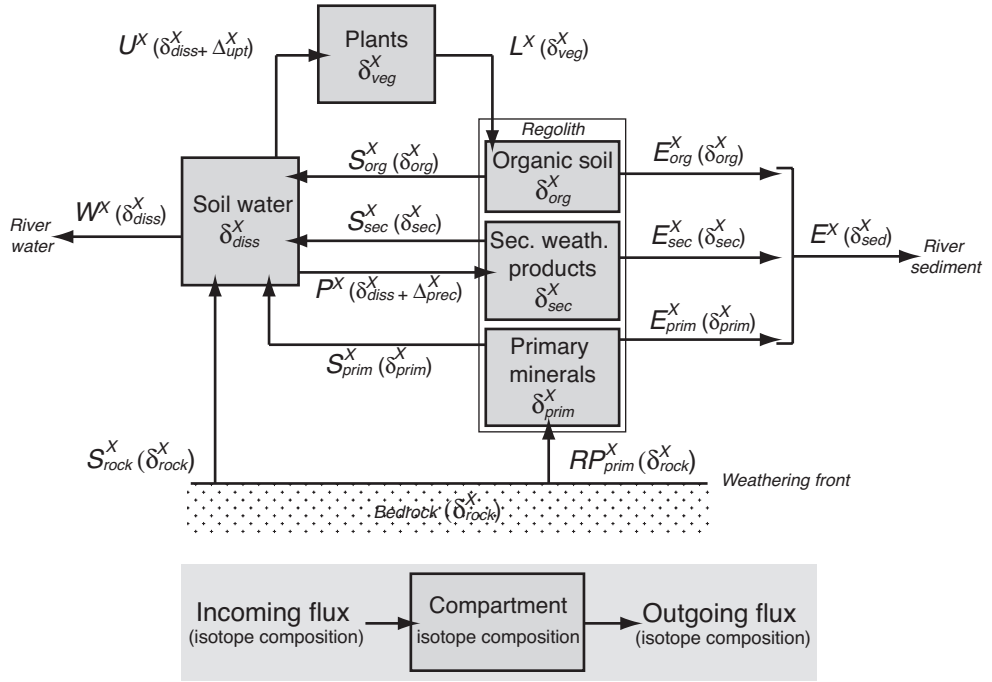

Fig. 1. Schematic diagram of the weathering zone model. See text and table 1 for symbols.

species. From this compartment plants take up their nutrients and weathering secondary products are precipitated. Finally, the vegetation compartment includes all tree roots and aboveground vegetation that is mainly higher plants (fig. 1). We treat the weathering zone as a "batch reactor," meaning that all compartments interact with one another in their entirety.

Topsoil is eroded away by soil creep, wind and rain splash. The products of these erosion processes represent mobilized material and form river sediment. Soil water is drained into rivers; the dissolved soil water species form the river dissolved load. Therefore, river dissolved and particulate loads reflect the export fluxes from the weathering zone. The model developed here conceptually represents a weathering system from the scale of a soil column to that of a large river.

In the following, the primary minerals, secondary weathering products, solid organic material, vegetation and soil water compartments are referred to using the subscripts *prim*, *sec*, *org*, *veg*, and *diss*, respectively.

The Steady-State Mass Balance

Throughout this study, we use the steady-state assumption that implies that in each compartment, over some time scale, incoming mass fluxes balance outgoing fluxes. This assumption holds for each element and for each isotope. Chemical elements enter the weathering zone by the passage of the unweathered material through the weathering front located by definition at the base of the regolith (Fletcher and others, 2006; Lebedeva and others, 2007). At steady-state, the regolith thickness remains constant, and the propagation of the weathering front occurs at a rate *RP* (for "regolith production") equal to that of material removal of regolith mass by physical erosion *E* and chemical weathering *W*, the sum of the two being defined as the denudation rate *D* (total mass, in kg m^{-2} yr^{-1}):

$$RP = E + W = D. \tag{1}$$

For a given metallic or metalloid element X (for example Li, Mg, Si, Ca), the propagation rate of the weathering front actually corresponds to the rate of regolith production RP times its concentration in bedrock, $[X]_{rock}$ (in mol kg^{-1}). Mineral dissolution at the weathering front results in a flux S^X_{rock} (for "solubilization"; elemental flux in mol m^{-2} yr^{-1}) from unweathered rock to soil water. Remaining primary minerals are transferred to the regolith, thereby generating a flux RP^X_{prim}. The element X is exported from the weathering zone either from the soil water compartment as dissolved species (net weathering flux W^X, sometimes referred to as "chemical erosion"; for example Ferrier and others, 2010) that eventually forms the river dissolved load, or from the regolith compartments as solid particles (erosion flux E^X) forming river sediment. Hence, the elemental steady-state mass balance for the whole weathering zone is:

$$S^X_{rock} + RP^X_{prim} = E^X + W^X = D \cdot [X]_{rock}. \tag{2}$$

Biological uptake is associated with an elemental flux U^X from the soil water compartment to the vegetation compartment, and litter fall L^X returns X, in a solid form, from plants to regolith. Secondary minerals and amorphous phases precipitate from solutes, and dissolved species adsorb onto mineral surfaces, resulting in an elemental flux P^X from the soil water compartment into the secondary weathering products compartment. Primary minerals, secondary weathering products, and solid organic material release X to the soil water compartment through dissolution, desorption, or leaching, grouped here under the term "solubilization" (S^X_{prim}, S^X_{sec}, and S^X_{org}). The regolith compartments supply solid material to river sediment through the elemental erosion fluxes E^X_{prim}, E^X_{sec}, and E^X_{org}. The sum of these three fluxes is E^X. The equations describing the balance between fluxes entering and leaving each compartment are:

$$\text{Regolith primary minerals} \quad RP^X_{prim} = E^X_{prim} + S^X_{prim} \tag{3a}$$

$$\text{Secondary precipitates} \quad P^X = E^X_{sec} + S^X_{sec} \tag{3b}$$

$$\text{Solid organic matter (plant litter)} \quad L^X = E^X_{org} + S^X_{org} \tag{3c}$$

$$\text{Vegetation} \quad U^X = L^X \tag{3d}$$

$$\text{Soil water} \quad S^X_{rock} + S^X_{prim} + S^X_{sec} + S^X_{org} = P^X + U^X + W^X. \tag{3e}$$

An isotope composition for the element X is now assigned to each of the five compartments (δ^X_{prim}, δ^X_{sec}, δ^X_{org}, δ^X_{veg}, and δ^X_{diss}, in ‰), to unweathered rock (δ^X_{rock}), and to bulk topsoil and river sediment (δ^X_{sed}). The δ symbol refers to the δ notation used in the literature to report stable isotope data relative to an international reference material (for example δ^7Li or δ^{26}Mg).

In our model, isotope fractionation is attributed to two fluxes: precipitation of secondary weathering products (P^X) and biological uptake (U^X). Indeed, several studies on metal stable isotopes in Earth surface processes point towards these two processes as being the most important in terms of isotope fractionation (for example Bullen and others, 2001; Pistiner and Henderson, 2003; Vigier and others, 2008; Black and others, 2008; von Blanckenburg and others, 2009; DePaolo, 2011). The two corresponding isotope fractionation factors are referred to here as Δ^X_{prec} and Δ^X_{upt} (expressed in ‰). We choose to use Δ^X, which is a permil expression of the α^X–isotope fractionation factor, with $\Delta^X \sim 10^3 \cdot (\alpha^X - 1)$, as Δ^X can be conveniently used in equations containing δ-values. We assume that no isotope fractionation occurs during

mineral dissolution. Steady-state equations can be written describing the balance between the isotope composition of fluxes entering and leaving each compartment of the weathering zone:

$$\text{Regolith primary minerals} \quad RP^X_{prim} \cdot \delta^X_{rock} = E^X_{prim} \cdot \delta^X_{prim} + S^X_{prim} \cdot \delta^X_{prim} \tag{4a}$$

$$\text{Secondary precipitates} \quad P^X \cdot (\delta^X_{diss} + \Delta^X_{prec}) = E^X_{sec} \cdot \delta^X_{sec} + S^X_{sec} \cdot \delta^X_{sec} \tag{4b}$$

$$\text{Solid organic matter (plant litter)} \quad L^X \cdot \delta^X_{veg} = E^X_{org} \cdot \delta^X_{org} + S^X_{org} \cdot \delta^X_{org} \tag{4c}$$

$$\text{Vegetation} \quad U^X \cdot (\delta^X_{diss} + \Delta^X_{upt}) = L^X \cdot \delta^X_{veg} \tag{4d}$$

$$\text{Soil water} \quad S^X_{rock} \cdot \delta^X_{rock} + S^X_{prim} \cdot \delta^X_{prim} + S^X_{sec} \cdot \delta^X_{sec} + S^X_{org} \cdot \delta^X_{org} = P^X(\delta^X_{diss} + \Delta^X_{prec}) + U^X(\delta^X_{diss} + \Delta^X_{upt}) + W^X \cdot \delta^X_{diss} \tag{4e}$$

$$\text{Whole weathering zone} \quad S^X_{rock} \cdot \delta^X_{rock} + RP^X_{prim} \cdot \delta^X_{rock} = E^X_{prim} \cdot \delta^X_{prim} + E^X_{sec} \cdot \delta^X_{sec} + E^X_{org} \cdot \delta^X_{org} + W^X \cdot \delta^X_{diss} = E^X \cdot \delta^X_{sed} + W^X \cdot \delta^X_{diss}. \tag{4f}$$

The Controls on the Isotope Composition of the Weathering Zone Compartments

The isotope composition of each compartment of the weathering zone can now be predicted as a function of fluxes and isotope fractionation factors by rearranging equations (3a) to (4e) (see Appendix A for details):

$$\text{Regolith primary minerals} \quad \delta^X_{prim} = \delta^X_{rock} \tag{5a}$$

$$\text{Secondary precipitates} \quad \delta^X_{sec} = \delta^X_{diss} + \Delta^X_{prec} \tag{5b}$$

$$\text{Solid organic matter (plant litter)} \quad \delta^X_{org} = \delta^X_{diss} + \Delta^X_{upt} \tag{5c}$$

$$\text{Vegetation} \quad \delta^X_{veg} = \delta^X_{diss} + \Delta^X_{upt} \tag{5d}$$

$$\text{Soil water} \quad \delta^X_{diss} = \delta^X_{rock} - \frac{E^X_{sec} \cdot \Delta^X_{prec} + E^X_{org} \cdot \Delta^X_{upt}}{S^X_{rock} + S^X_{prim}}. \tag{5e}$$

Equations (5a) to (5e) illustrate and quantify the dependence of isotope composition in the compartments of the weathering zone on both isotope fractionation factors and fluxes. Equation (5a) prescribes that the composition of the primary minerals remaining in the regolith is identical to that of bedrock, provided that isotope fractionation during mineral dissolution is absent. Equations (5b) and (5c) describe that at steady-state, the isotope composition of the regolith's secondary weathering products and of the vegetation are offset from that of soil water by the respective isotope fractionation factor. Finally, equations (5c) and (5d) describe that the isotope composition of the vegetation is identical to that of the regolith organic material at steady-state.

The way the isotope composition of soil water and river water, δ^X_{diss}, is set is more complex since both biological uptake and precipitation of secondary weathering products affect this compartment. However, understanding the factors controlling δ^X_{diss} is essential, as the isotope composition of plants, solid organics and secondary weathering products are simply offset from that of water by the relevant fractionation factors (eqs 5b to 5c). Three parameters set the isotope composition of soil water or river water (eq 5e):

(i) The two fractionation factors Δ^X_{prec} and Δ^X_{upt}. However, isotope ratios of dissolved species are governed by the combined effects of the two processes, and their values depend on the relative weight of these two isotope fractionation factors.

(ii) The erosion fluxes E^X_{sec} and E^X_{org}. Following equations (3b) and (3c), at steady-state these fluxes also correspond to net formation of secondary products ($P^X - S^X_{sec}$) and of solid organic material ($L^X - S^X_{org}$). Importantly, E^X_{sec} and E^X_{org} can be very small for example in slow-eroding systems, in which case the isotope composition of water is predicted to be close to that of bedrock, regardless of the magnitude of the isotope fractionation factors involved. This is because the dissolved species can carry a distinct isotope signature only if the "fractionated" solid material, be it plant litter or clay minerals, is exported out of the system. Otherwise, if the element X is released again to water rather than exported as solids, its isotope composition in water will tend to be that of the bedrock.

(iii) The supply of the element X to soil water from primary mineral dissolution, which occurs both at the weathering front during regolith production (S^X_{rock}) and throughout the regolith (S^X_{prim}). If the sum of these two fluxes ($S^X_{rock} + S^X_{prim}$) is large, the effect of isotope fractionation by secondary precipitate formation and plant uptake will be minimal, because the supply of material to soil water with a bedrock isotope composition will dominate its isotope composition. On the contrary, if the supply to soil water by primary mineral dissolution is low, large isotope differences are expected between rock and soil water.

We show below how these three processes quantitatively control the isotope composition of soil water and river water, and hence of all the compartments of the weathering zone. In the next section, we discuss the assumptions the model is based on and their implications.

DISCUSSING AND TESTING THE MODEL ASSUMPTIONS

The model developed here relies on a number of assumptions. Before exploring the model results, we review these assumptions, discuss their validity, and where possible suggest ways to test them and to adapt sampling strategies suited to provide the parameters required to constrain the model.

The Steady-State Assumption

The model assumes steady-state, meaning that in each compartment, incoming and outgoing fluxes are balanced. First, although the steady-state assumption does not realistically describe fast-changing systems (for example soil development over previously glaciated settings or a significant shift in vegetation driven by climate change), systems changing slowly compared to the residence time of the considered element in different compartments can be considered as being at quasi steady-state. This quasi steady-state characteristic makes these systems tractable with the model. Furthermore, the mass balance equations laid out in this work can also be used for non steady-state scenarios if time-derivative terms are added to equations (1) to (4f). However, in this case additional assumptions are required as the terms for fluxes need to be parameterized as a function of time or other variables, such as the mass of the element in the compartments (for example using first-order kinetics). The resulting set of mass balance equations will most likely need to be solved numerically. With the steady-state assumption we can solve the mass balance equations algebraically and determine explicit expressions of the isotope composition of the compartments (eqs 5a to 5e).

For the entire weathering zone and for the regolith compartments, the steady-state assumption is likely justified on time scales corresponding to the residence time of chemical elements in the weathering zone (typically from 10^3 to 10^5 yrs). For individual internal compartments, such as soil water or vegetation, element residence times are shorter and steady-state is most likely attained over shorter time scales. However, fluctuations around the steady-state are expected. Indeed, significant temporal and spatial variability is observed in the isotopic composition of soil water at the

seasonal and inter-annual times scales (for example Tipper and others, 2010a; Lemarchand and others, 2010; Bolou-Bi and others, 2012). The temporal variability observed in the dissolved load of small rivers (Georg and others, 2006; Tipper and others, 2012a) likely reflects, at first-order, variable regolith layers from which water is preferentially tapped through time (Calmels and others, 2011). However, temporal changes in processes are also possible (Tipper and others, 2012a). To be used in conjunction with the present model, soil water and river water samples need to be time-integrated or need to be at least representative with respect to temporal variability. Temporal variability is likely to affect solid export as well, depending on the temporal variability in the erosion processes involved. Moreover, the isotopic composition of river sediment is likely to show variability if different grain size fractions are considered, in particular for elements which are strongly affected by secondary mineral formation or by adsorption (Lemarchand and others, 2012). In this case, the time-dependent transport capacity affecting river channels might introduce further temporal variability in sampled river sediment (Bouchez and others, 2011), and this effect has to be circumvented through analysis of multiple grain sizes (Lemarchand and others, 2012), or of river sediment depth-profiles (dos Santos Pinheiro, 2013).

The validity of the steady-state assumption can be tested in various ways, among which the most obvious is the direct measurement of elemental fluxes into, from, and within the weathering zone. Such a test requires knowing the total mass fluxes such as water discharge, erosion, or litter fall, and in theory can be carried out at both the regolith and river scales. For example, denudation rates and river fluxes in a tropical catchment in Puerto Rico show that equation (2) holds true there, and hence that weathering operates at steady-state (White and others, 1998; Turner and others, 2003).

In addition, isotope ratios can be used to further test the steady-state assumption. A first possibility to test the model prediction is to investigate whether the isotope composition of the vegetation and of the regolith organic material are identical at steady-state (eqs 5c and 5d). Another possibility is to test for steady-state for the whole weathering zone (eq 4f). For example, the study by Ziegler and others (2005b) on Si isotopes in Puerto Rico can be combined with the Si fluxes reported by White and others (1998) and Turner and others (2003) to perform this test from the scale of the regolith to that of the small river basin (table 2). According to the values of $D \cdot [Si]_{rock}$ (White and others, 1998) and W^{Si} (Turner and others, 2003), about 50 percent of the Si is exported as dissolved matter in this setting (table 2). Using the Si isotope composition of bulk soil and river water reported by Ziegler and others (2005b), equation (4f) predicts that δ^{Si}_{rock} is around 0 permil, which is in reasonable agreement with the isotope composition of bulk rock, −0.2 permil, reported by Ziegler and others (2005b). At present, further tests of this type at the river scale are impaired by the absence of accurate sediment fluxes in most isotope geochemical studies. A crude estimate of the elemental fluxes can be calculated using suspended sediment concentration in river water, and element concentration in sediment and in water. Only a few studies report such data on both suspended sediment concentration and isotope composition in river dissolved and particulate loads (at the small river scale in Iceland and Greenland: Pogge von Strandmann and others, 2006, 2008, 2010; Wimpenny and others, 2010a, 2011; and at the large river scale on the Mackenzie and Changjiang basins: Lemarchand and Gaillardet, 2006; Chetelat and others, 2009; Millot and others, 2010; Tipper and others, 2012b). However, testing the steady-state hypothesis from these datasets remains difficult first because most studies do not report the isotope composition of the source material that is required to constrain δ^{X}_{rock}. Second, variable isotope composition for suspended load and bedload are reported throughout these studies, which would have to be accounted for to constrain a grain size-integrated δ^{X}_{sed}. Finally, all of these studies rely on a single sample of river water

Table 2

Si fluxes and isotope composition in the Luquillo catchment. Puerto Rico

Parameter	*Value*	*Reference*
Weathering front propagation rate = denudation rate (m Myr^{-1})	58	White and others (1998)
SiO_2 concentration in unweathered diorite (%)	61.2	White and others (1998)
Rock density (kg m^{-3})	2,700	
$\delta^{Si}_{rock} + RP^{Si}_{prim}$ (mol m^{-2} yr^{-1})	1.59	
Dissolved Si river flux (10^{-9} mol m^{-2} s^{-1})	25.6	Turner and others (2003)
W^{Si} (mol m^{-2} yr^{-1})	0.81	
River δ^{30}Si during baseflow (‰)	1.4	Ziegler and others (2005b)
River δ^{30}Si during stormflow (‰)	0.6	Ziegler and others (2005b)
δ^{Si}_{diss} (‰)	1.0	
Bulk top soil δ^{30}Si (‰)	-0.9	Ziegler and others (2005b)
δ^{Si}_{sed} (‰)	-0.9	
Bulk rock δ^{30}Si (‰)	-0.2	Ziegler and others (2005b)

rather than on time series, such that potential temporal variability in the isotope composition of dissolved material cannot be assessed to constrain δ^{X}_{diss}. The effects of the uncertainties in δ^{X}_{rock}, δ^{X}_{sed}, and δ^{X}_{diss} on the weathering zone mass balance are assessed quantitatively later in this paper.

Spatially Homogenous Compartments

The model does not entail any vertical stratification of the regolith compartments, although such a stratification is commonly observed in soils studies (Kisakürek and others, 2004; Cividini and others, 2010; Lemarchand and others, 2010; Tipper and others, 2010a; Lemarchand and others, 2012; Pogge von Strandmann and others, 2012; Huang and others, 2012). Since the solid regolith compartments (*sec*, *org*, and *prim*) supply sediment to rivers, the relevant material to be sampled and analyzed is that being eroded from the regolith column, meaning topsoil in most environments. For soil water it is likely that the layer preferentially supplying metals to the river dissolved load varies seasonally following changes in hydrological conditions. In order to obtain a representative isotope composition of the dissolved load at the scale of a soil column, depth-profiles of soil water should be sampled, and the layer being drained to rivers should be identified.

Unlike what is assumed in the model, the various components of the vegetation compartment (*veg*, that is roots, wood stem, bark, branches, and leaves) exhibit different isotope composition (for example Guelke and others, 2007; Holmden and Bélanger, 2010; Cobert and others, 2011). This means that vegetation samples need to be averaged over these main components to be used with our model, for example using so-called allometric equations (Holmden and Bélanger, 2010). Moreover, as litter fall returns mostly leaves and small branches to the soil pool, it does not always yield the same isotope composition as the bulk above-ground vegetation. This might introduce an "apparent" isotope fractionation during litter fall, which is not catered for by the model developed here. In this case, the value for δ^{X}_{veg} needs to be constrained by independent information on the actually recycled vegetation compartments. How-

ever, over sufficiently long time scales, all elements taken up by vegetation should eventually be returned to the regolith, through a combination of litter fall and root decay.

River Material as Probes of Soil Weathering Processes

Export of solutes and particles out of the weathering system to rivers occurs through purely advective processes (drainage, erosion) and shall not result in mass-dependent isotope fractionation of metals. We therefore assume that the isotope composition of river dissolved and particulate load reflects that of soil water and topsoil, respectively. This will be true only if biological activity and precipitation of secondary weathering products are negligible during transport from the weathering zone to the sampling point along the river, which is not always the case (Hughes and others, 2011). It is expected that the larger the river, the more significant these additional processes will become. Yet if the river element fluxes fulfill the steady state mass balance, river samples are still representative of the integral over all biogeochemical processes in the basin, up to the sampling point. In this case, the apparent isotope fractionation factor governing the isotope composition of river dissolved and particulate loads will not only reflect the soil processes, but also processes occurring during the transport, such as equilibration between a dissolved species and its adsorbed counterpart. The impact of such processes can for example be detected by sampling river water at different locations following a longitudinal transect, or using time series sampling at a given location (Hughes and others, 2011).

Furthermore, weathering reactions can also occur along deep fractures and in groundwater systems, which will most likely result in isotope signatures that differ from those acquired in soils. The different pathways of river water and dissolved load can for example be deconvolved using chemical and isotopic tracers (Calmels and others, 2011).

The Absence of Atmospheric Sources of Metals to the Weathering Zone

We assume that only rock dissolution at the weathering front supplies metal to the weathering zone. Importantly, precipitation (rain, snow), dust, or groundwater, can also deliver metals to the weathering system. The fluxes associated with non-weathering inputs have to be estimated. If they are significant, their isotope composition must be determined and taken into account in the model by adapting the value of δ^X_{rock}, which is then a flux-weighted average of the bedrock-derived and the additional inputs, or by correcting the measured value of δ^X_{diss}.

The Absence of Isotope Fractionation During Mineral Dissolution

In the model, "apparent" isotope fractionation during rock weathering is taken into account in the form of secondary products precipitation (P^X and Δ^X_{prec}). However, we assume that no metal stable isotope fractionation takes place during dissolution of primary minerals or secondary weathering products, during desorption, or when cations are leached from plant litter. These assumptions hold true under the following conditions: (1) the different source materials undergoing dissolution, leaching, or desorption do not differ from each other in their isotope composition and (2) isotope fractionation does not occur during desorption or dissolution itself.

Regarding condition (1) and the dissolution of primary minerals (fluxes S^X_{rock} and δ^X_{prim}), it has been shown that the variability in isotope composition of different primary minerals in igneous rocks is relatively small compared to the variability produced by weathering reactions at the Earth surface (Hindshaw and others, 2011; Tipper and others, 2012a). Exceptions to this rule have been reported, such as Li (Richter and others, 2003; Lundstrom and others, 2005; Parkinson and others, 2007), Mg (Handler and others, 2009; Pogge von Strandmann and others, 2011), Si (Ziegler and others,

2005a; Savage and others, 2012), or Sr (Charlier and others, 2012). Moreover, we acknowledge that the presence of clay minerals or carbonates in sedimentary source rocks might introduce more heterogeneity as compared to the case of igneous source rocks. In the regolith, condition (1) will not be fulfilled if several generations of secondary weathering products with distinct isotope signatures dissolve at different rates.

Concerning condition (2), for a given mineral, steady-state dissolution dictates that the isotopic composition of released element is the same as that of bulk mineral, once a surface layer of a necessarily limited thickness has been weathered. In other words, the outer layer of the mineral that undergoes dissolution cannot be depleted indefinitely in one given isotope. This conceptual argument is supported by most of the time-resolved dissolution experiments on basalts (Ziegler and others, 2005b; Wimpenny and others, 2010a; Ryu and others, 2011; Verney-Carron and others, 2011) showing the absence of isotope fractionation after a relatively short initial period during which the lightest isotope is preferentially released. However, significant isotope fractionation was recorded for Fe during the initial phase of experiments of hornblende dissolution by siderophores (Brantley and others, 2004), ligand-controlled and reductive goethite dissolution (Wiederhold and others, 2006), ligand-controlled dissolution of biotite and chlorite (Kiczka and others, 2010); and for Mg in magnesite batch dissolution experiment (Pearce and others, 2012). Desorption can also be associated with isotope fractionation (Huang and others, 2012). Despite these potential complications, we consider at first-order that no fractionation occurs during dissolution at steady-state. However, such an isotope fractionation effect could in principle be incorporated into the model equations (eqs 4b, 4c, and 4e).

Representing Multiple Fractionation Processes by a Single Isotope Fractionation Factor

Isotope fractionation in the model relies on two processes, namely precipitation of secondary weathering products and biological uptake. The associated isotope fractionation factors of the two individual processes, Δ^X_{prec} and Δ^X_{upt}, can represent either equilibrium or kinetic isotope fractionation. Most likely, however, Δ^X_{prec} and Δ^X_{upt} are rate-dependent and thus represent a combination of both equilibrium and kinetic fractionation (DePaolo, 2011). Δ^X_{prec} and Δ^X_{upt} might also lump the effects of several physico-chemical reactions that would be associated with their own isotope fractionation factor. For example, mass-dependent isotope fractionation between soil water and bulk plants might result from the combination of (1) isotope fractionation during root absorption or by symbiotic fungi (2) translocation through the cell membrane and within the plant (for example von Blanckenburg and others, 2009; Cobert and others, 2011). Similarly, if several dissolved chemical species exist in solution (as an acid-base or redox couple, for example), isotope fractionation between the bulk dissolved pool and the solid soil can arise from the combination between (1) isotope fractionation between the dissolved species (for example $B(OH)_3$—$B(OH)_4^-$ or $Fe(H_2O)_6^{2+}$—$Fe(H_2O)_6^{3+}$; Welch and others, 2006; Klochko and others, 2006); (2) fractionation between one of these species and the solid phase that precipitates (Skulan and others, 2002; Lemarchand and others, 2005). Finally, several parallel processes might contribute to the fractionation effect: uptake into different plant species will potentially be associated with distinct isotope fractionation factors (Guelke and others, 2007; Bolou-Bi and others, 2010; Cobert and others, 2011), and precipitation of different solid products will be associated with a variety of distinct isotope fractionation factors (for example for Fe: Anbar and others, 2005; Johnson and others, 2005). The resulting observed isotope fractionation will depend on the relative contribution of these different processes to the total flux of X from soil water to plants or to solid soil. As long as the sampling is representative for the different weathering

zone compartments, the associated isotope fractionation factors that can be inferred will reflect the result of these relative contributions.

Treating the Weathering Zone as a Batch Reactor

In our model weathering system, we assume that the whole pool of dissolved species (soil water or river water) interacts with homogenous regolith or river sediment compartments. In other words, our zero-dimensional "batch reactor" model does not account for reactions occurring along flowpaths. Such reactions can lead to Rayleigh effects if the residual compartment is not allowed to interact further with the new compartments, for example if soil water is isolated from secondary precipitate after precipitation. The validity of this assumption and its consequences on the predictions that can be drawn from the model are discussed in the next section.

PREDICTING THE ISOTOPE COMPOSITION OF THE WEATHERING ZONE COMPARTMENTS

Using our model, we set out to predict (1) how the isotope composition of the weathering zone compartments varies as a function of the respective elemental fluxes, (2) in what weathering system the most distinct isotope signatures are detectable, and (3) which compartment is best-suited in order to trace present and past weathering processes. We use the equations derived above (eqs 5a to 5e) to make these predictions in the form of a sensitivity analysis on δ^X_{diss}. To do so we quantify how the isotope composition of soil water varies with the relative fluxes and associated isotope fractionation factors. To facilitate this sensitivity analysis, equation (5e) is first rendered non-dimensional. This step is necessary to make the different isotope systems comparable. First, fluxes into and from the weathering zone can vary between zero and very large values, depending on the element and setting. As it is the rate at which the element is supplied to the regolith that directly or indirectly sets the pace of the processes occurring in the weathering zone, normalizing to this flux allows us to present the range of possible fluxes in a comparable manner. Second, isotope fractionation for a given element also depends on the relative mass difference between the isotopes. The range of isotope compositions observed in weathering systems hence varies from 50 permil (^{7}Li/^{6}Li) to less than a 1 permil (^{88}Sr/^{86}Sr). Since we aim at developing a model valid for the entire set of novel stable isotope systems, our predictions in terms of isotope compositions have to be normalized to a metric that reflects the overall range of isotope compositions attainable by each system. In the following, these normalized parameters are described.

Normalizing Element Fluxes to the Rate of Passage through the Weathering Front

The rate at which the element X is supplied to the regolith is the flux that ultimately determines the pace of all other transfers within the weathering zone. Hence it is convenient to normalize all the other fluxes to $S^X_{rock} + RP^X_{prim} = D \cdot [X]_{rock}$, which is the flux at which the element X passes through the weathering front at the base of the regolith. Furthermore, a series of measurable parameters known in the weathering literature, such as the chemical depletion fraction (*CDF*) or the elemental mass transfer coefficient (τ), are by definition fractions of the flux of matter crossing the weathering front. Therefore, the normalized fluxes are defined as:

$$f^X = \frac{F^X}{S^X_{rock} + RP^X_{prim}} = \frac{F^X}{D \cdot [X]_{rock}} \tag{6}$$

where F^X (upper case) is any dimensional flux and f^X (lower case) is its non-dimensional counterpart. For most fluxes, f^X will be lower than 1. For example, only a fraction of X crossing the weathering front will be dissolved from primary minerals or remain unaltered (s^X_{rock}, rp^X_{prim}, s^X_{prim}) or exported as dissolved species or solids (w^X, e^X,

e^X_{prim}, e^X_{sec}, and e^X_{org}). However, s^X_{sec}, s^X_{org}, p^X, u^X, and l^X can all be higher than 1, and reflect the cycling of the element X within the weathering zone. The value of s^X_{sec} actually corresponds to the number of times X is cycled between secondary precipitates and the dissolved compartment before it leaves the weathering zone. Similarly, the value of s^X_{org} corresponds to the number of times X is cycled through the vegetation compartment.

Lumping the Isotope Fractionation Factors

Isotope ratios in soil water and river water are the results of the combined effects of the two main processes that fractionate isotopes and their respective isotope fractionation factors Δ^X_{prec} and Δ^X_{upt}. A "lumped isotope fractionation factor" can be defined if we first weigh the two individual fractionation factors by their respective erosion fluxes (or equivalently by their net formation rate, eqs 3b and 3c):

$$\bar{\Delta}^X = \frac{E^X_{sec} \cdot \Delta^X_{prec} + E^X_{org} \cdot \Delta^X_{upt}}{E^X_{sec} + E^X_{org}}. \tag{7}$$

$\bar{\Delta}^X$ will attain values between those of Δ^X_{prec} and Δ^X_{upt}, depending on the erosion fluxes E^X_{sec} and E^X_{org}. Using this definition of a lumped isotope fractionation factor, it is now convenient to recast equation (5e) in the form:

$$\delta^X_{diss} = \delta^X_{rock} - \bar{\Delta}^X \cdot \frac{E^X_{sec} + E^X_{org}}{S^X_{rock} + S^X_{prim}}. \tag{8}$$

The flux-weighted average of the two isotope fractionation factors is thus a controlling factor not only on the magnitude, but also on the direction of isotope fractionation. However, in some settings, certain elements are sensitive mostly to biological uptake (this can be the case for Ca) or to precipitation of secondary weathering products or adsorption, respectively (for example Li in most cases). In this case, the generic formulation of equation (8) will be replaced by simpler expressions, as discussed later. Importantly, equation (8) makes the distinction between the effect of isotope fractionation itself ($\bar{\Delta}^X$) and the effect of pure mass balance, recast as the ratio between erosion of fractionated solids to primary mineral dissolution, $(E^X_{sec} + E^X_{org})/(S^X_{rock} + S^X_{prim})$. Note that equation (8) predicts that $(\delta^X_{diss} - \delta^X_{rock})$ and $\bar{\Delta}^X$ have opposite signs, consistent with the fact that soil water is being depleted in the isotope favored by $\bar{\Delta}^X$, while the regolith compartments will be enriched in that isotope.

Exploring the Isotope Fractionation Space

The way isotope ratios vary with fluxes in the weathering system can now be quantitatively explored. Using the definition in equation (6), equation (8) can be recast as:

$$\frac{\delta^X_{diss} - \delta^X_{rock}}{\bar{\Delta}^X} = \frac{e^X_{sec} + e^X_{org}}{r p^X_{diss} + w^X_{prim}}. \tag{9}$$

The normalized difference between isotope ratios $(\delta^X_{diss} - \delta^X_{rock})/\bar{\Delta}^X$ expresses the isotopic difference between soil water or river water, and bedrock, normalized to the flux-weighted average isotope fractionation factor of the system, $\bar{\Delta}^X$. For example, if the left hand term in equation (9) is equal to 0.5, it means that the difference in isotope composition between soil water and bedrock, in permil, will be half of the flux-weighted average isotopic fractionation factor at play in the weathering zone. This normalized difference in isotope composition is equal to the ratio between (1) the export of solid, isotopically-fractionated material ($e^X_{sec} + e^X_{org}$) and (2) the total (that is at the weathering front plus in the regolith) flux of dissolution of primary minerals ($S^X_{rock} + S^X_{prim}$).

Given that the net incorporation of X into solid organic material or secondary weathering products in the regolith cannot exceed its dissolution from primary minerals ($e^X_{sec} + e^X_{org}$) is necessarily lower than ($s^X_{rock} + s^X_{prim}$). This has an important implication: in our model weathering zone, the normalized isotope difference ($\delta^X_{diss} - \delta^X_{rock}$)/$\bar{\Delta}^X$ cannot be greater than 1 in absolute value (eq 9). In other words, the maximum isotope differences that can be observed between bedrock and water is equal to the average isotope fractionation factor $\bar{\Delta}^X$. An exception to this prediction arises when Rayleigh-type processes markedly enrich one isotope in a residual compartment. These processes occur when an isotope is strongly depleted when fluids move along reactive flowpaths. Rayleigh-type mass balances have been used to explain isotope data in the weathering zone (for example Rudnick and others, 2004; Thompson and others, 2007; Tipper and others, 2012a). Our model does not cater for such effects, as it envisages the weathering zone as a "batch reactor." We see this assumption as reasonable in many natural systems as it is expected that two processes will counteract Rayleigh effects occurring along reaction pathways: (1) continuous dissolution of primary minerals S^X_{prim} which supply the solution with X at an isotope composition δ^X_{rock}, and (2) dissolution of "fractionated" products S^X_{sec} and S^X_{org}, which returns isotopically fractionated X to the solution. Through these processes, ($\delta^X_{diss} - \delta^X_{rock}$) is maintained closer to what is expected from the "batch" reactor model than if only Rayleigh-type processes were operating. The presence of Rayleigh-type processes can be evaluated through the examination of reported values for ($\delta^X_{diss} - \delta^X_{rock}$). According to equation (9), this difference should not exceed the lumped isotope fractionation factor $\bar{\Delta}^X$ in absolute value. We compiled δ^X_{diss} values from the literature for Li, B, Mg, Si, and Ca dissolved in soil water, ground water, and river water (Appendix B). Where possible, we corrected δ^X_{diss} for non-weathering inputs, and estimated δ^X_{rock} in order to calculate ($\delta^X_{diss} - \delta^X_{rock}$). The distributions of δ^X_{diss} and ($\delta^X_{diss} - \delta^X_{rock}$) are plotted in figure 2 and compared with values of isotope fractionation factors derived from experimental studies. For Si and Ca, and to a lesser extent for B and Li, most of the data plot between 0 permil and the range defined by the reported values of Δ^X_{prec} and Δ^X_{upt}, consistent with what is predicted by the model. These observations show that the framework proposed here is at first-order applicable to most natural settings, despite its relative simplicity. Interestingly, figure 2 also shows that for Li, B, Mg, and Si, most of the ($\delta^X_{diss} - \delta^X_{rock}$) are different from 0, suggesting that for these elements ($e^X_{sec} + e^X_{org}$) is higher than 0 (eq 9). This is not the case for Ca, despite the fact that most Δ^{Ca}_{prec} and Δ^{Ca}_{upt} values are different from 0, thus implying that most Ca is exported from the global weathering zone as dissolved species.

The normalized isotope difference ($\delta^X_{diss} - \delta^X_{rock}$)/$\bar{\Delta}^X$ is plotted in figure 3 as a function of the sum of the non-dimensional erosion fluxes ($e^X_{sec} + e^X_{org}$) and the sum of the non-dimensional dissolution fluxes ($s^X_{rock} + s^X_{prim}$). At low values of ($e^X_{sec} + e^X_{org}$), a large fraction of X is exported as primary minerals or as dissolved material. In this case, ($\delta^X_{diss} - \delta^X_{rock}$)/$\bar{\Delta}^X$ is low (eq 9, fig. 3), or, in other words, the isotope composition of the dissolved compound is close to that of bedrock, since no significant amount of X is exported as "fractionated" solid. The highest absolute value of ($\delta^X_{diss} - \delta^X_{rock}$)/$\bar{\Delta}^X$ is 1, in which case δ^X_{diss} approaches ($\delta^X_{rock} - \bar{\Delta}^X$). This value is obtained when ($e^X_{sec} + e^X_{org}$) $\sim$ ($s^X_{rock} + s^X_{prim}$) (1:1 line in fig. 3). This case occurs when most of the X unlocked from primary minerals is exported as fractionated solids, be it in secondary weathering products or in the form of solid organic material.

The close inspection of equation (9) shows how the weathering regime of a given setting can control the extent of isotope fractionation. Indeed, the ratio ($e^X_{sec} + e^X_{org}$)/($s^X_{rock} + s^X_{prim}$) is likely to be high in settings and for elements for which erosion processes dominate over weathering of primary minerals. A large degree of isotope fractionation is expected in this case. Conversely, if removal of solid, isotopically fractionated material is

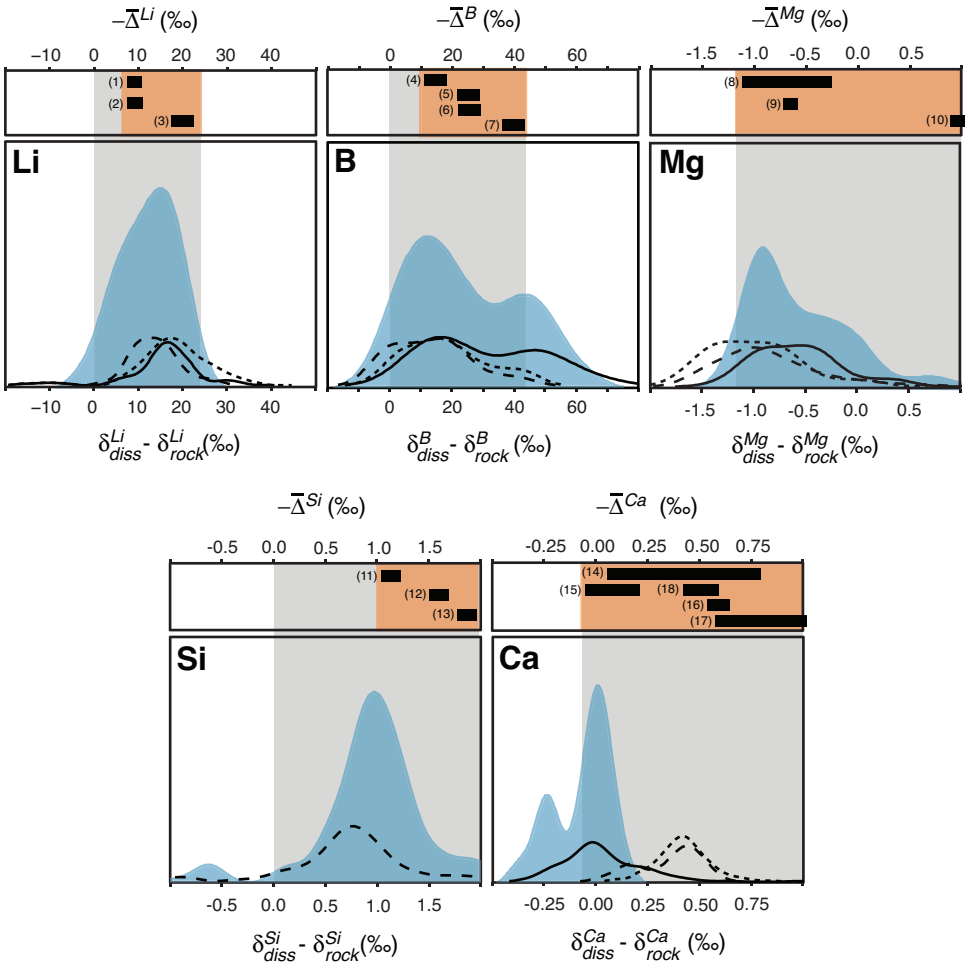

Fig. 2. Distributions (probability density functions) of isotope composition of soil water, ground water, and river water (large panels, δ^{X}_{diss} and $\delta^{X}_{diss} - \delta^{X}_{rock}$) and weathering-related isotope fractionation factors (small panels, $-\Delta^{X}_{prec}$ and $-\Delta^{X}_{upt}$) compiled from the literature, for the novel stable isotope systems δ^{7}Li, δ^{11}B, δ^{26}Mg, δ^{30}Si, and $\delta^{44/42}$Ca (Appendix B). Large panels: color-filled blue curves are distributions of ($\delta^{X}_{diss} - \delta^{X}_{rock}$) data corrected for "external inputs" (rain, dust, and anthopogenic inputs and evaporite weathering). These curves thus reflect silicate weathering for B, Li and Si, and both silicate and carbonate weathering for Ca and Mg. As both corrections for external inputs and estimates of δ^{X}_{rock} introduce significant uncertainties (Appendix B), also plotted for comparison are non-corrected δ^{X}_{diss} data (dotted curves), external inputs-corrected δ^{X}_{diss} data (stippled curves) and non-corrected ($\delta^{X}_{diss} - \delta^{X}_{rock}$) data (solid curves). In these diagrams, the vertical scale is arbitrary. Small panels: range of published isotope fractionation factors (1) co-precipitation of Li into calcite at 5 to 30 °C (Mariott and others, 2004); (2) incorporation of Li into smectite at 25 to 90 °C (Vigier and others, 2008); (3) incorporation of Li into basalt during seafloor weathering (Chan and others, 1992); (4) adsorption of B onto birnessite at 25 °C, pH < 8 (Lemarchand and others, 2007); (5) adsorption of B onto Mississippi sediment (Spivack and others, 1987); (6) adsorption of B onto humic acids at 25 °C, 5 < pH < 9 (Lemarchand and others, 2005); (7) adsorption of B onto goethite at 25 °C, pH < 8 (Lemarchand and others, 2005); (8) uptake of Mg by rye grass and clover (Bolou-Bi and others, 2010); (9) uptake of Mg by wheat (Black and others, 2008); (10) co-precipitation of Mg into calcite at 26.5 °C (Saulnier and others, 2012); adsorption of Si onto (11) goethite and (12) ferrihydrite (Delstanche and others, 2009); (13) uptake of Si by bamboo (Ding and others, 2009); (14) precipitation of Ca as calcite at 25 °C, rate-dependent (DePaolo, 2011); adsorption of Ca onto (15) montmorillonite, (16) illite, and (17) kaolinite in seawater at 21 °C (Ockert and others, 2013); (18) uptake of Ca by beans (Cobert and others, 2011). Importantly, these isotope fractionation factors are not derived from field studies on continental weathering studies, such that there is no redundancy of data between the large and the small panels. For each of the isotope system, the best estimate of the lumped isotope fractionation factor $-\bar{\Delta}^{X}$ lies in the range defined by these process-specific fractionation factors, and is given by the orange area. The light gray area extending over both small and large panels is the range of ($\delta^{X}_{diss} - \delta^{X}_{rock}$) values predicted by our model (eq 9), that is between 0 and $-\bar{\Delta}^{X}$.

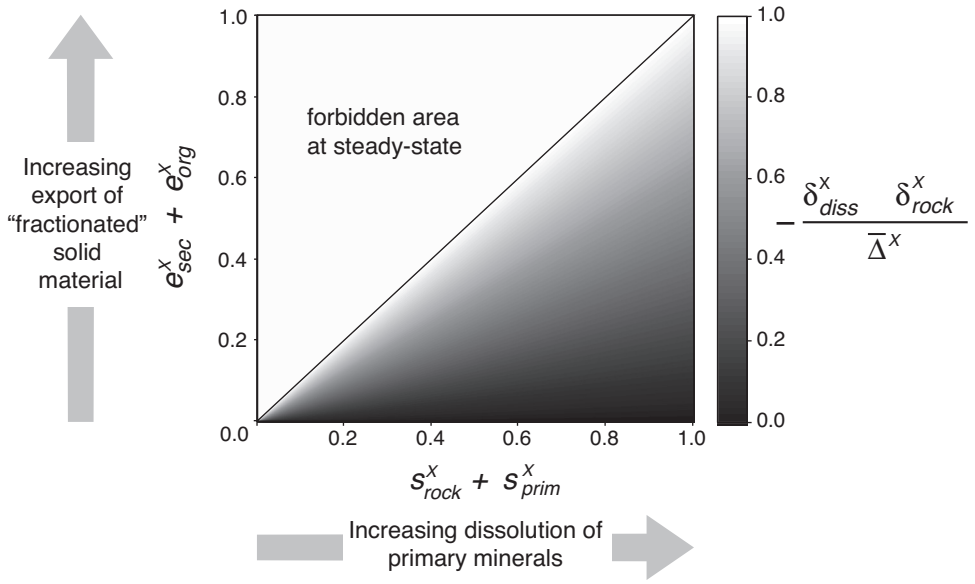

Fig. 3. Relative isotope difference $\frac{\delta^X_{diss} - \delta^X_{rock}}{\bar{\Delta}^X}$ (eq 9) as a function of $(s^X_{rock} + s^X_{prim})$ (proportion of X dissolved at the weathering front and within the regolith) and $(e^X_{sec} + e^X_{org})$ (proportion of X exported as solid secondary weathering products or as solid organics). White corresponds to the highest difference in isotope composition observable between rock and dissolved compounds, at steady-state. In this case this difference is equal to the lumped isotope fractionation factor $\bar{\Delta}^X$ (eq 7). Black corresponds to the case where there is no difference in isotope composition between rock and dissolved compounds. Note that the value on the Y-axis $(e^X_{sec} + e^X_{org})$ cannot exceed, at steady-state, that on the X-axis $(s^X_{rock} + s^X_{prim})$, since X needs to be unlocked from primary minerals before being incorporated (and hence undergo isotope fractionation) into solid secondary weathering products or into organic matter. This condition implies the existence of a "forbidden area".

not effective as compared to the weathering of primary minerals, small extents of isotope fractionation are predicted by the model. This control on isotope composition by the relative magnitudes of the fluxes is similar to the "reservoir effect" suggested by Tipper and others (2012b) to explain the Li and Mg isotope data in the Mackenzie basin, and to the conclusion derived by Chetelat and others (2009) from the study of B isotopes in the Changjiang basin. In the last section of this paper, the model is applied to trace past weathering regimes from the Li isotope sedimentary record.

Application of the Model to the Examples of Ca and Li Isotopes

While considering a lumped isotope fractionation factor $\bar{\Delta}^X$ is a requirement for modeling isotope systems in a general way, we can consider specific cases in which isotope fractionation is governed exclusively either by the formation of secondary precipitates or by plant uptake. In these cases, only one fractionation factor matters. Two examples are treated here:

(1) Ca ($^{44}Ca/^{42/40}Ca$), which in a number of settings will not be incorporated into secondary minerals but will be markedly affected by plant uptake (Wiegand and others, 2005; Cenki-Tok and others, 2009; Holmden and Bélanger, 2010; Cobert and others, 2011; Hindshaw and others, 2011). This might not be true in arid settings (Ewing and others, 2008) or when carbonate precipitation occurs, such as commonly observed at the river scale (Tipper and others, 2008a).

(2) Li ($^7Li/^6Li$), which is relatively insensitive to biological activity but is mostly controlled by precipitation of clay minerals and by adsorption onto mineral surfaces

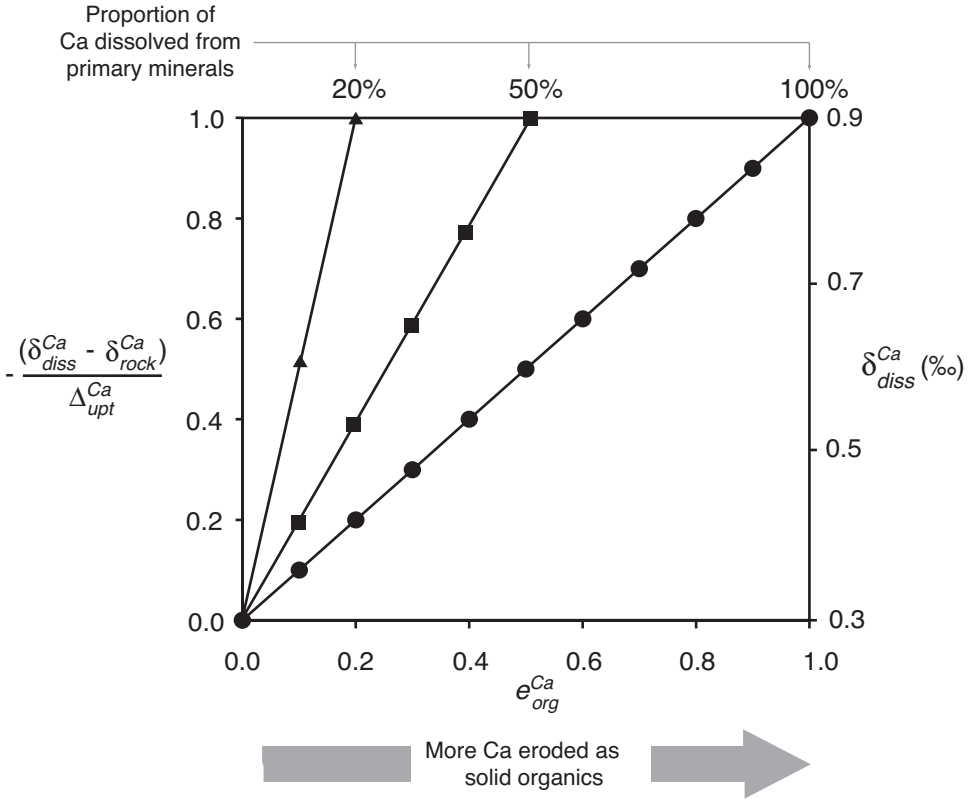

Fig. 4. Relative isotope fractionation of Ca (eq 10) as a function of e^{Ca}_{org} (proportion of Ca exported as solid organic, X-axis), for 3 different proportions of Ca released from primary minerals ($s^{Ca}_{rock} + s^{Ca}_{prim}$, upper X-axis labels). On the right Y-axis, the resulting isotope composition of soil water is indicated, assuming δ^{Ca}_{rock} of 0.3‰ and Δ^{Ca}_{upt} of −0.6‰.

(Pistiner and Henderson, 2003; Huh and others, 2004; Kisakurek and others, 2004; Vigier and others, 2008; Lemarchand and others, 2010).

Using equation (9), the isotope composition of soil water or river water, δ^{X}_{diss}, for these two elements is:

$$\frac{\delta^{Ca}_{diss} - \delta^{Ca}_{rock}}{\Delta^{Ca}_{upt}} = -\frac{e^{Ca}_{org}}{s^{Ca}_{rock} + s^{Ca}_{prim}} \tag{10}$$

$$\frac{\delta^{Li}_{diss} - \delta^{Li}_{rock}}{\Delta^{Li}_{prec}} = -\frac{e^{Li}_{sec}}{s^{Li}_{rock} + s^{Li}_{prim}}. \tag{11}$$

The behavior of Ca isotope composition in soil water or river water in the weathering zone following equation (10) is plotted in figure 4. The extent of Ca fractionation increases linearly with the proportion of Ca eroded after dissolution from primary minerals and incorporation into biomass. Ca fractionation reaches its maximum extent ($\delta^{Ca}_{diss} - \delta^{Ca}_{rock} = -\Delta^{Ca}_{upt}$) when all Ca dissolved from primary minerals is exported as solid organic matter. This is likely to happen, for example, in moderately-fast denuding granitic settings where Ca is mostly hosted in plagioclase. Indeed, in this case, the soil residence time is sufficiently long so that all Ca is released from

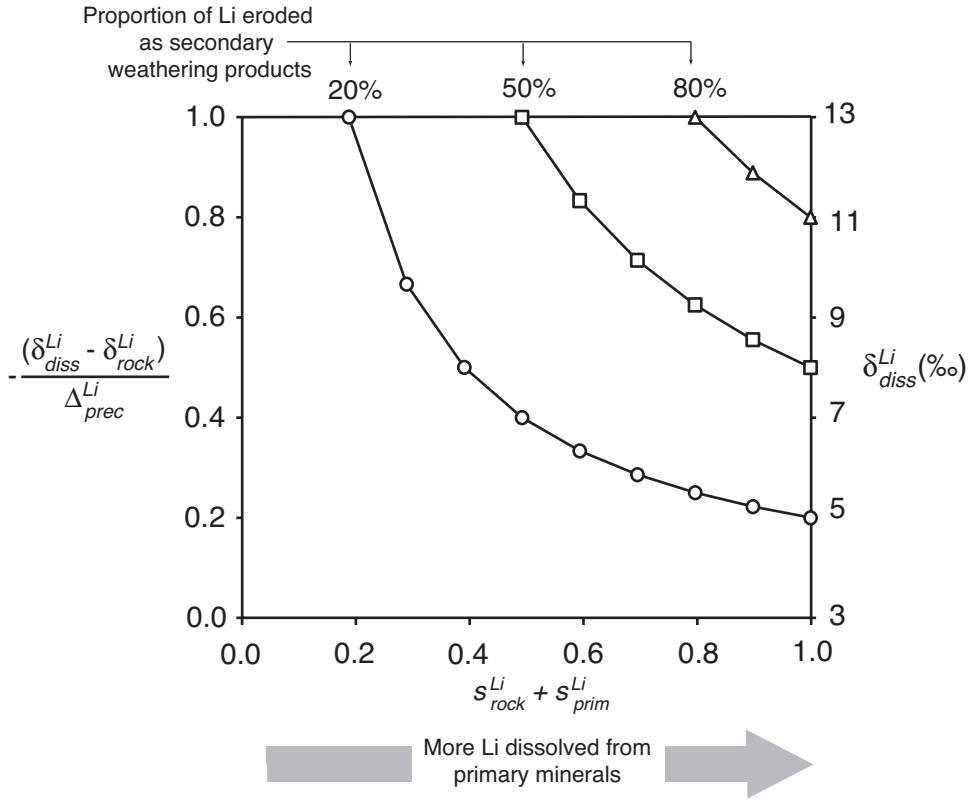

Fig. 5. Relative isotope fractionation of Li (eq 11) as a function of $s^{Li}_{rock} + s^{Li}_{prim}$ (proportion of Li released from primary minerals, X-axis), for 3 different proportions of Li exported as secondary weathering products (e^{Li}_{sec}, upper labels). On the right Y-axis, the resulting isotope composition of soil water is indicated, assuming δ^{Li}_{rock} of 3‰ and Δ^{Li}_{prec} of −10‰.

plagioclase, a mineral with relatively fast dissolution kinetics (Brantley and others, 2008). However, erosion of topsoil maintains a significant export of Ca in solid organic particles leading to strongly fractionated δ^{Ca}_{diss}. In settings where denudation is slower, for example in tropical shields, all Ca from plagioclase will be released too, but because of long soil residence times, it is also likely that most Ca will be leached from plant litter before it is eroded away.

The behavior of the Li isotope composition in soil water or river water as a function of the proportion of primary mineral dissolution (eq 11) is shown in figure 5. The extent of Li isotope fractionation relative to bedrock decreases with increasing proportion of Li released from primary minerals, for a given proportion of Li exported as secondary precipitates (for example oxides or clays) or adsorbed onto mineral surfaces. The maximum extent of fractionation ($\delta^{Li}_{diss} - \delta^{Li}_{rock} = -\bar{\Delta}^{Li}_{prec}$) is attained when the export of secondary precipitates is equal to the proportion of Li dissolved from primary minerals. This is unlikely to happen in very slowly denuding systems, even if all Li is released from primary minerals, because Li, once incorporated into secondary precipitates, is likely to be released to soil water before the precipitate is eroded away. High extents of fractionation between soil water and rock are however possible in fast to moderately fast denuding settings, provided that soil water chemistry and dynamics permit the precipitation of all Li from soil water, so that almost no Li is exported as

dissolved species. The behavior of Li isotopes during weathering, and the link between Li isotope ratio and weathering regime are discussed in the last section of this paper.

We have shown in this section how the presented model can be used to predict under which conditions the signatures of novel stable isotope systems will be strongest, and how they vary quantitatively with element fluxes, provided that the relevant isotope fractionation factors are known. In the next section, we show how the model can be practically used in an "inverse way" to calculate isotope fractionation factors from the isotope compositions of the weathering zone compartments, and from elemental fluxes or concentrations.

CALIBRATING ISOTOPE FRACTIONATION FACTORS FROM FIELD MEASUREMENTS

Although isotope fractionation factors can be measured in experimental studies or calculated from atomistic modeling, the applicability of these isotope fractionation factors might be hampered by the complexity of natural settings as compared to simple experimental set ups and the competing effects of kinetic and equilibrium fractionation (DePaolo, 2011). Such issues can be circumvented by calibrating isotope fractionation factors on materials sampled in the field.

Equation (9) relates the observable isotope fractionation to the underlying fluxes. In those cases where the fluxes operating in the weathering zone are known by other means, the measured isotope ratios can serve to calibrate isotope fractionation factors from field data. For example, the combination of cosmogenic nuclides and mass balances directly quantifies denudation and weathering rates in weathering zones over granitic lithology (for example Riebe and others, 2004). Such rates can also be inferred from river dissolved and particulate fluxes. However, it is also possible to express the predicted isotope ratios in the weathering zone as a function of measured element concentrations only. First, the non-dimensional erosion fluxes in equation (9) can be written:

$$e^X_{sec} = \frac{E^X_{sec}}{D \cdot [X]_{rock}} = \frac{E \cdot [X]_{sec}}{D \cdot [X]_{rock}} = (1 - CDF)\frac{[X]_{sec}}{[X]_{rock}} \tag{12}$$

$$e^X_{org} = \frac{E^X_{org}}{D \cdot [X]_{rock}} = \frac{E \cdot [X]_{org}}{D \cdot [X]_{rock}} = (1 - CDF)\frac{[X]_{org}}{[X]_{rock}} \tag{13}$$

where $[X]_{sec}$ corresponds to the concentration of X carried by secondary weathering products in topsoil or river sediment (that is mass of X_{sec} divided by mass of soil or sediment) and $[X]_{org}$ is the concentration of X in topsoil or river sediment carried by solid organic material. *CDF* is the chemical depletion fraction as defined by Riebe and others (2001, 2004) and which indexes the overall mass loss occurring during weathering and export of dissolved compounds. *CDF* varies between 0 (no weathering) and 1 (total rock dissolution), but most commonly attains maximum values of 0.5 in granitic lithologies, since the parent rock contains weathering-resistant minerals such as quartz and insoluble elements such as Fe and Al, that precipitate as clay minerals and oxi-hydroxides. *CDF* can be calculated using the enrichment of an immobile element during weathering X_i (for example Zr, Ti, Nb) in the weathered material as compared to the concentration of this element in parent material:

$$CDF = 1 - \frac{[X_i]_{rock}}{[X_i]_{reg}} \tag{14}$$

where $[X_i]_{reg}$ is the concentration of X_i in the bulk regolith. In practice, $[X]_{sec}$ can be accessed after sequential extractions of topsoil (for example through extraction of Fe-Mn-Al oxy-hydroxides using mild HCl and then a reducing agent, followed by clay

separation using settling methods; for example Wiederhold and others, 2007a; Guelke and others, 2010). Similarly, $[X]_{org}$ can be extracted by selective extraction of the organic material using hydrogen peroxide, for example.

Second, the flux related to primary dissolution in equation (9), ($s^X_{rock} + s^X_{prim}$) also has to be expressed as a function of element concentrations. This flux actually corresponds to a fractional mass loss of X from primary minerals as compared to bedrock. To quantify this process, we define here τ^X_{prim}, which can be calculated from the concentrations of X and X_i in the parent material and topsoil or river sediment, following:

$$s^X_{rock} + s^X_{prim} = \frac{S^X_{rock} + S^X_{prim}}{D \cdot [X]_{rock}} = -\tau^X_{prim} = 1 - \frac{[X]_{prim}}{[X]_{rock}} \cdot \frac{[X_i]_{rock}}{[X_i]_{reg}}. \quad (15)$$

Although the definition of τ^X_{prim} is similar to that of the elemental mass transfer coefficient τ by Chadwick and others (1990), τ^X_{prim} indexes the amount of X lost from primary minerals only, whereas values of τ reported in the literature in contrast relate to the net effect of combined mineral dissolution and precipitation, and thus to the net loss or gain of X. Finally, the isotope composition of soil water in equation (9) can now be calculated as a function of chemical concentrations only (eqs 12, 13, and 14):

$$\frac{\delta^X_{diss} - \delta^X_{rock}}{\bar{\Delta}^X} = \frac{1 - CDF}{\tau^X_{prim}} \cdot \frac{[X]_{sec} + [X]_{org}}{[X]_{rock}} = -\frac{[X]_{sec} + [X]_{org}}{[X_i]_{reg} \cdot \left(\frac{X}{X_i}\right)_{rock} - [X]_{prim}}. \quad (16)$$

Equation (16) shows how isotope fractionation factors, isotope ratios in the weathering zone, and weathering chemical indexes are linked. This relationship also emphasizes that the compartment-specific concentrations $[X]_{sec}$, $[X]_{org}$ and $[X]_{prim}$ need to be measured rather than X bulk concentration in the regolith or in river sediment. To do so, sequential extractions or grain size-specific analyses have to be carried out (Wiederhold and others, 2007a, 2007b; Poitrasson and others, 2008; Guelke and others, 2010; Holmden and Bélanger, 2010; Hindshaw and others, 2011; Bolou-Bi and others, 2012; Tipper and others, 2012b). Furthermore, if the considered element is influenced by both precipitation of secondary weathering products and uptake by plants, the isotope fractionation factor that can be calculated from ($\delta^X_{diss} - \delta^X_{rock}$) reflects the weighted average of these two categories of processes, $\bar{\Delta}^X$ (eq 7). For the respective isotope fractionation factors to be told apart, the isotope composition of secondary precipitates (δ^X_{sec}) and of organic matter or plants (δ^X_{org} or δ^X_{veg}) have to be measured as well. Then, equations (5b) to (5d) can be used to infer the individual values of Δ^X_{prec} and Δ^X_{upt}.

Altogether, our analysis provides the necessary constraints, for example, to guide sampling towards the compartments in which the most prominent isotope signatures will be obtained, if the element fluxes are known. In the following, we explore how the steady-state mass balance can be used to retrieve information on element fluxes even if only bulk topsoil or river sediment and soil water or river water are measured, and even if isotope fractionation factors are not known.

Exporting Fractionated Material: The Links between Isotope Ratios and Weathering and Erosion Fluxes

In all cases discussed above, a process dominating isotope fractionation will enrich some isotopes in the regolith or sediment and depleted these isotopes in the dissolved species. When recast as relative isotope ratios, only mass balance affects these isotope enrichments and depletions. The isotope fractionation factor itself does not affect this partitioning.

The relationship between the ratio of solid-to-dissolved export of *X*, E^X/W^X (or equivalently the fraction of *X* exported as dissolved species, w^X) and the isotope ratios in the weathering system compartments, can be obtained by combining equations (2) and (4f):

$$\frac{\delta^X_{diss} - \delta^X_{rock}}{\delta^X_{sed} - \delta^X_{rock}} = -\frac{E^X}{W^X} = -\frac{1 - w^X}{w^X}. \tag{17}$$

Indeed, equation (17) does not feature any isotope fractionation factor, thus showing that the ratio between the isotope composition of river water and bulk sediment (with bedrock isotope composition as a reference) is not dependent upon the internal processes of the system (biological uptake and precipitation of secondary products of weathering), but rather on the relative magnitudes of the two export fluxes E^X and W^X. During riverine transport, an element X can be transferred between the solid and the dissolved load. If this transfer also entails isotope fractionation, both E^X/W^X and the isotope composition of the river dissolved and particulate loads are modified, but the validity of equation (17) is not affected.

The parameters E^X/W^X and w^X reflect the geochemical solubility of *X* in a given setting or in other words an element-specific weathering intensity. The relationship described by equation (17) is plotted in figure 6. The largest differences in isotope composition between the dissolved and solid phases are obtained when the export of *X* is greatly in favor of one or the other types of export. For example, if w^X is equal to 0.8 (hence $e^X = 1 - w^X$ is equal to 0.2, meaning that 80% of *X* is exported as solutes), then $(\delta^X_{sed} - \delta^X_{rock})$ is, in absolute value, four times larger than $(\delta^X_{diss} - \delta^X_{rock})$.

Equation (17) can also be used as a check of the steady-state hypothesis from measurements of the isotope composition of bulk river sediment, river water and bedrock, provided that the dissolved and sediment fluxes for *X* are known. We performed this test on the Luquillo catchment, Puerto Rico, already mentioned earlier in the discussion of the steady-state assumption. Equation (17) can also be used to calculate the proportion of dissolved export of an element *X* in a weathering system, provided that the isotope composition of the river dissolved and particulate loads and of bedrock are known. Rearranging equation (17) yields:

$$w^X = \frac{\delta^X_{sed} - \delta^X_{rock}}{\delta^X_{sed} - \delta^X_{diss}}. \tag{18}$$

Equation (18) can be used (1) at the soil scale using soil water draining the soil column along with topsoil; (2) at the river scale using river dissolved and particulate material; (3) in the oceanic or lacustrine sedimentary record using the authigenic and detrital phases, allowing for determination of past solid-to-dissolved export ratios. Such an approach does not require knowing the isotope fractionation factors involved. However, at all scales, the determination of w^X from equation (18) carries an uncertainty. Practically, this uncertainty will result from:

(1) The uncertainty in the rock isotope composition, δ^X_{rock}. Large uncertainties in δ^X_{rock} could arise in small river basins, where representative bedrock might be difficult to sample, and in large river basins if lithologies with different isotope ratios contribute to the element X in the river.

(2) The uncertainty in water isotope composition, δ^X_{diss}. In rivers, this uncertainty might arise from a temporal variability in δ^X_{diss}, which is not accounted for by the sampling frequency. This issue is the largest at the soil scale, where uncertainty is introduced from the vertical variability in δ^X_{diss} in soil water that cannot be easily integrated.

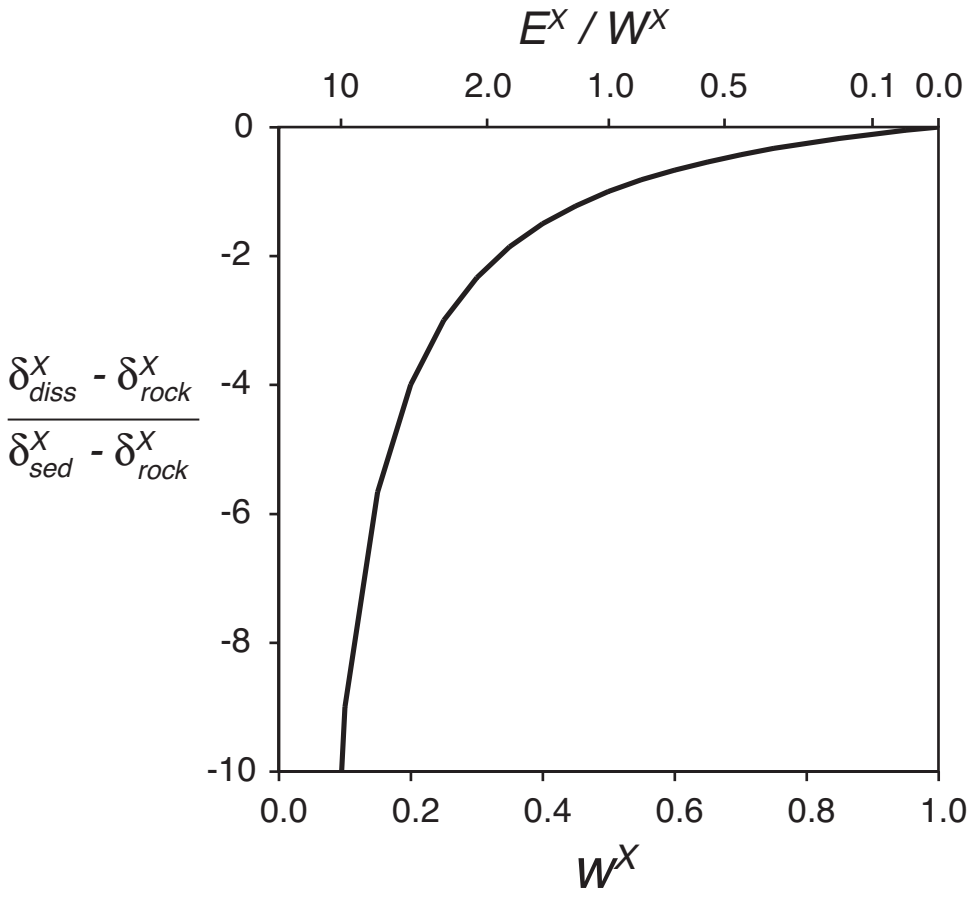

Fig. 6. Ratio of the differences in isotope composition between a dissolved element in soil water or river water and bedrock, to that between the same element in river sediment or topsoil and bedrock, as a function of the fraction of dissolved export w^X (lower X-axis) and the ratio of the elemental erosion flux E^X to the weathering flux W^X (upper X-axis).

(3) The uncertainty in the erosion products' isotope composition, δ^X_{sed}. At the soil scale, topsoil is the exported material in most cases, and will accurately yield the value of δ^X_{sed}. However, in rivers and especially in large rivers, hydrodynamic sorting will result in large uncertainties in δ^X_{sed} if the grain size-dependence is not accounted for.

(4) The value of w^X. For example, it is expected that in low-w^X settings, where most of the export of X is accommodated by the sediment, δ^X_{sed} will be very close to δ^X_{rock}. This will tend to make the denominator in equation (17) close to 0 and will magnify the effects of uncertainties in isotope ratios listed above.

We can quantitatively assess these issues through uncertainty propagation. This uncertainty estimation is done here for the typical case of a small river; calculations and hypotheses are explained in detail in Appendix C, and results are plotted in figure 7. The absolute uncertainty in w^X will be the largest in river basins where w^X is either high (>0.85) or low (<0.15). This translates to very high relative uncertainties in w^X ($>50\%$) for low w^X settings and to high relative uncertainties in $e^X = 1 - w^X$ ($>50\%$) for high-w^X settings. The domain where the most precise prediction of both w^X and e^X can be done is when w^X is between 0.20 and 0.80. This would exclude, in most settings,

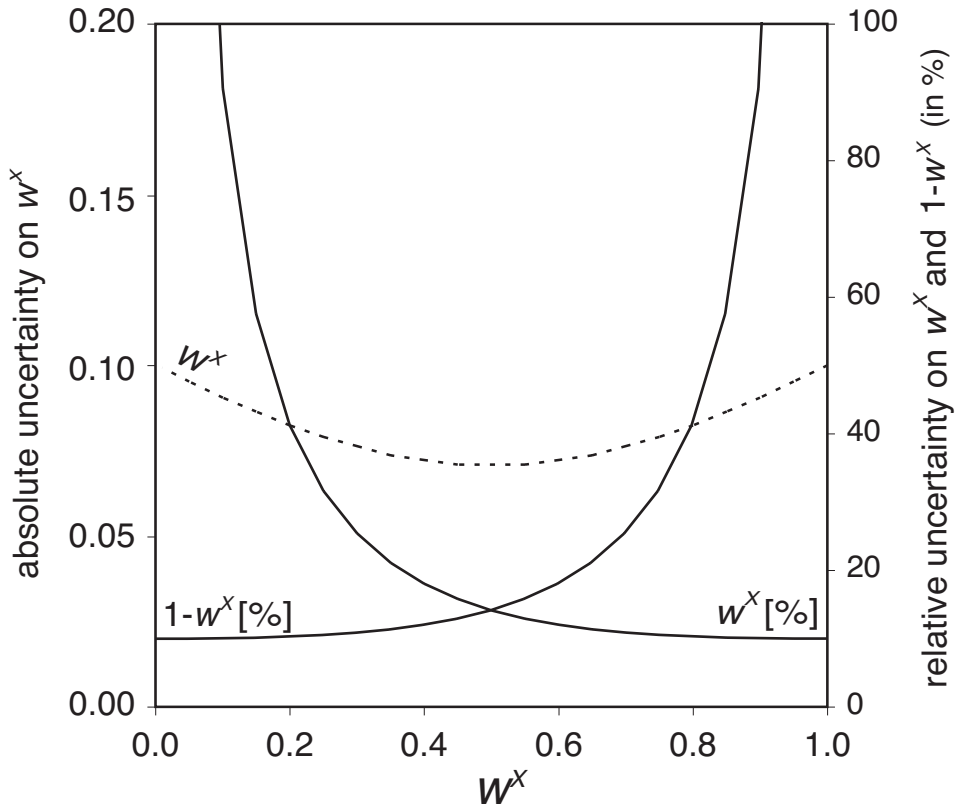

Fig. 7. Absolute (stippled line) and relative (solid lines) uncertainties on the proportion of dissolved export of *X*, w^X, and the proportion of particulate export, $1 - w^X$, calculated from isotope compositions of river material (dissolved and particulate) and source rock, as a function of w^X. The absolute uncertainty in w^X is identical to that in $1 - w^X$. Details of the calculations and hypotheses are given in Appendix B. Uncertainty on source rock isotope composition δ^X_{rock} was assumed to be 0. Important parameters of this uncertainty propagation (Appendix B) are the ratios between (1) the uncertainty on δ^X_{diss} and on δ^X_{sed}; (2) the difference $(\delta^X_{sed} - \delta^X_{diss})$. Here these ratios are equal to 0.1, following data reported in the literature for small river on Mg and Li isotopes. This figure is thought to be representative of the uncertainties to be encountered at the small river scale, although uncertainties on the source isotope composition (δ^X_{rock}) would uniformally shift the uncertainty curves towards higher values.

elements that are very soluble, like Ca, or elements which are poorly soluble like Li, which is strongly affected by adsorption onto particulate matter. This would also exclude extreme geomorphic regimes: those where denudation rates are so low and soil residence times are so long that most metals are leached from solids and subsequently exported as dissolved species; but also those settings where soil residence time is too short to allow significant release of metals to the dissolved phase. Nevertheless, outside of these boundaries, the simple fact that either of the compartments has an isotope composition close to that of the bedrock already has a straightforward, qualitative implication in that this compartment is the main carrier of *X* out of the weathering zone.

Disclosing past geomorphic regimes from the sedimentary record: the example of Li isotopes

There is a growing interest in using the sedimentary record of novel stable isotopes to infer past weathering regimes. Recently, a palaeo-seawater Li isotope curve

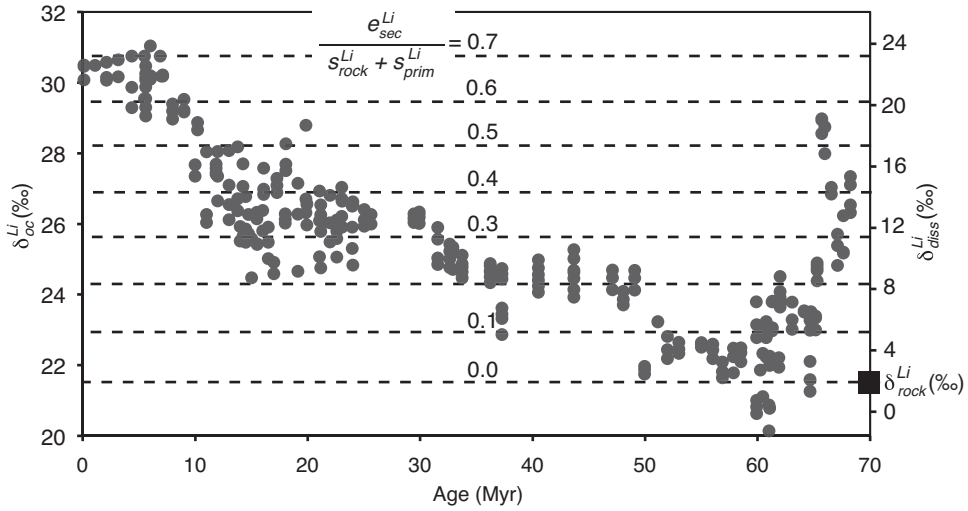

Fig. 8. Li stable isotope record in the ocean from Misra and Froelich (2012) and weathering conditions on the continents through the Cenozoic. All parameters are represented by the same set of data points, only axes change, since the different parameters are linearly related. Left axis: Li isotope composition for the oceans (δ^{Li}_{oc}) as measured in foraminifera (Misra and Froelich, 2012). Right axis: corresponding values for Li isotope composition of the global river dissolved load (δ^{Li}_{diss}) derived from an ocean mass-balance (Appendix D; Misra and Froelich, 2012). Stippled lines: corresponding value of the ratio between Li export as secondary weathering products (e^{Li}_{sec}) and Li released from primary minerals ($s^{Li}_{rock} + s^{Li}_{prim}$), calculated following equation (11), and assuming that δ^{Li}_{diss} from the ocean mass-balance is equivalent to δ^{Li}_{diss} of the model.

was reported for the Cenozoic (up to 68 Myrs ago) by Misra and Froelich (2012), derived from $^{7}Li/^{6}Li$ ratios measured in planktonic foraminifera (fig. 8). The shift in oceanic $\delta^{7}Li$ of +9 permil over the last 60 Myrs was interpreted to represent an increase in the $^{7}Li/^{6}Li$ ratio of dissolved riverine Li. This increase was in turn suggested to reflect a change of the global continental weathering regime with time. Oceanic $\delta^{7}Li$ at −60 Myrs are closer to those of the upper continental crust, which supposedly reflects a higher contribution of areas of "congruent" weathering that is without net formation of secondary precipitates. A progressively increasing contribution of settings where clays and oxides are formed, and thereby preferentially retain the light Li isotope into solids, would then explain the rise in the river and ocean Li isotope ratio.

In this section, we quantitatively revisit Misra and Froelich (2012)'s record using our model, and in particular we use equation (11) in order to generate a curve of the relative fluxes of Li (primary mineral dissolution and erosion of secondary weathering products) in the global weathering zone. This curve is then tentatively interpreted in terms of the prevailing denudation and weathering regime in the past, by parameterizing the Li isotope weathering signature using the steady-state denudation-weathering model developed by Ferrier and Kirchner (2008).

Variations of Relative Weathering Fluxes in the Past

Following the approach of Misra and Froelich (2012), the Li isotope composition of river water through the Cenozoic was modeled using assumptions on oceanic Li concentration and isotope mass balances (Appendix D, fig. 8). Riverine Li isotope composition (δ^{Li}_{diss}) is calculated to be around 0 to 5 permil between −60 and −50 Myrs, and then increases almost linearly to the present value of about 22 permil (fig. 7). Using equation (11), the ratio between the export flux of Li as secondary precipitates to Li release flux from primary mineral dissolution can be calculated,

provided that the associated isotope fractionation factors are known at the time of export.

First, we estimate present-day dissolved Li fluxes into the oceans to be between 10 and 50 percent of total Li transported by rivers (Martin and Meybeck, 1979; Gaillardet and others, 2003; Viers and others, 2009). A reasonable estimate for the global scale is 30 percent. This means that the ratio $e^{Li}_{sec}/(s^{Li}_{rock} + s^{Li}_{prim})$ is equal to 0.7. This number corresponds to a maximum estimate, as it ignores that river sediment could also transport Li hosted in primary minerals. We further assume that river sediments do not release nor scavenge Li upon entry into the ocean, so that all riverine dissolved Li reaches the open ocean. We can now use equation (8) together with estimates of the fractionation factor Δ^{Li}_{prec} to assess whether this number is accurate for the modern weathering regime. Given that the present-day global $(\delta^{Li}_{diss} - \delta^{Li}_{rock})$ is around 20 permil (as can be read from fig. 7), equation (8) yields that the global Δ^{Li}_{prec} is −30 permil or lower. This number is larger than the isotope fractionation factor of Li incorporation into smectite at 25 °C, which has been estimated to be −10 permil from laboratory experiments (Vigier and others, 2008). The fractionation factor for Li adsorption onto gibbsite has been determined to be −13 permil (Pistiner and Henderson, 2003). However, a value of about −20 permil was reported for the incorporation of Li during oceanic crust weathering by Chan and others (1992). Large fractionation factors values, for example associated with Li incorporation into iron oxides, were suggested by Millot and others (2010) to explain Li isotope data from the Mackenzie River basin. Our estimate suggests that at the global scale, yet unidentified processes are fractionating Li isotopes during weathering, or that a large kinetic effect is superimposed onto an equilibrium process, such as Li adsorption onto solid surfaces or incorporation into oxides or clays. Nevertheless, in the following we use 0.7 as the present value for the ratio $(e^{Li}_{sec}/(s^{Li}_{rock} + s^{Li}_{prim}))$, implying a Δ^{Li}_{prec} of −30 permil.

Once the ratio $(e^{Li}_{sec}/(s^{Li}_{rock} + s^{Li}_{prim}))$ of the modern weathering regime is known, the variation of this flux ratio through the past can be computed. We assume here, following Misra and Froelich (2012), that (1) the isotope fractionation factor Δ^{Li}_{prec} is constant throughout this interval and (2) the isotope composition of the crust undergoing weathering, δ^{Li}_{rock}, is constant. The results of this calculation are represented by the stippled contour lines in figure 8. They show that the fraction of Li exported to the ocean as secondary minerals was 0 percent 60 Myrs ago when $\delta^{Li}_{diss} \sim \delta^{Li}_{rock}$. Later, this fraction rose steadily throughout the Cenozoic up to 6 Myrs ago. At first sight, our quantitative findings support the qualitative interpretation of Misra and Froelich (2012) in that the global weathering regime switched from a "congruent" to a "non-congruent" mode. The most likely geologic explanation is that global erosion rate increased at the cost of the global weathering rate. However, this conclusion is solely based on a mass balance approach. Recent concepts on how weathering fluxes and intensities evolve when denudation rates change make use of mineral dissolution and precipitation kinetics. We proceed to evaluate the Li isotope composition in the weathering zone in the light of those models.

Placing Paleo-Seawater Li Isotopes into Past Geomorphic Regimes

Explaining differences in Li isotope compositions between the weathering zone compartments as a function of the geomorphic regime requires knowing how changes in denudation rate shift (1) isotope fractionation factors and (2) relative fluxes of Li between compartments. Knowing both allows the prediction of the normalized difference in isotope ratios $(\delta^{Li}_{diss} - \delta^{Li}_{rock})/\bar{\Delta}^{Li}_{prec}$, as a function of the denudation rate. Geomorphic regimes can be characterized by one end-member featuring long regolith residence time under low denudation rates, where the weathering intensities are at their maximum and the weathering fluxes are limited by the supply of unweathered material at the weathering front ("supply-limited" regime; Riebe and others, 2004;

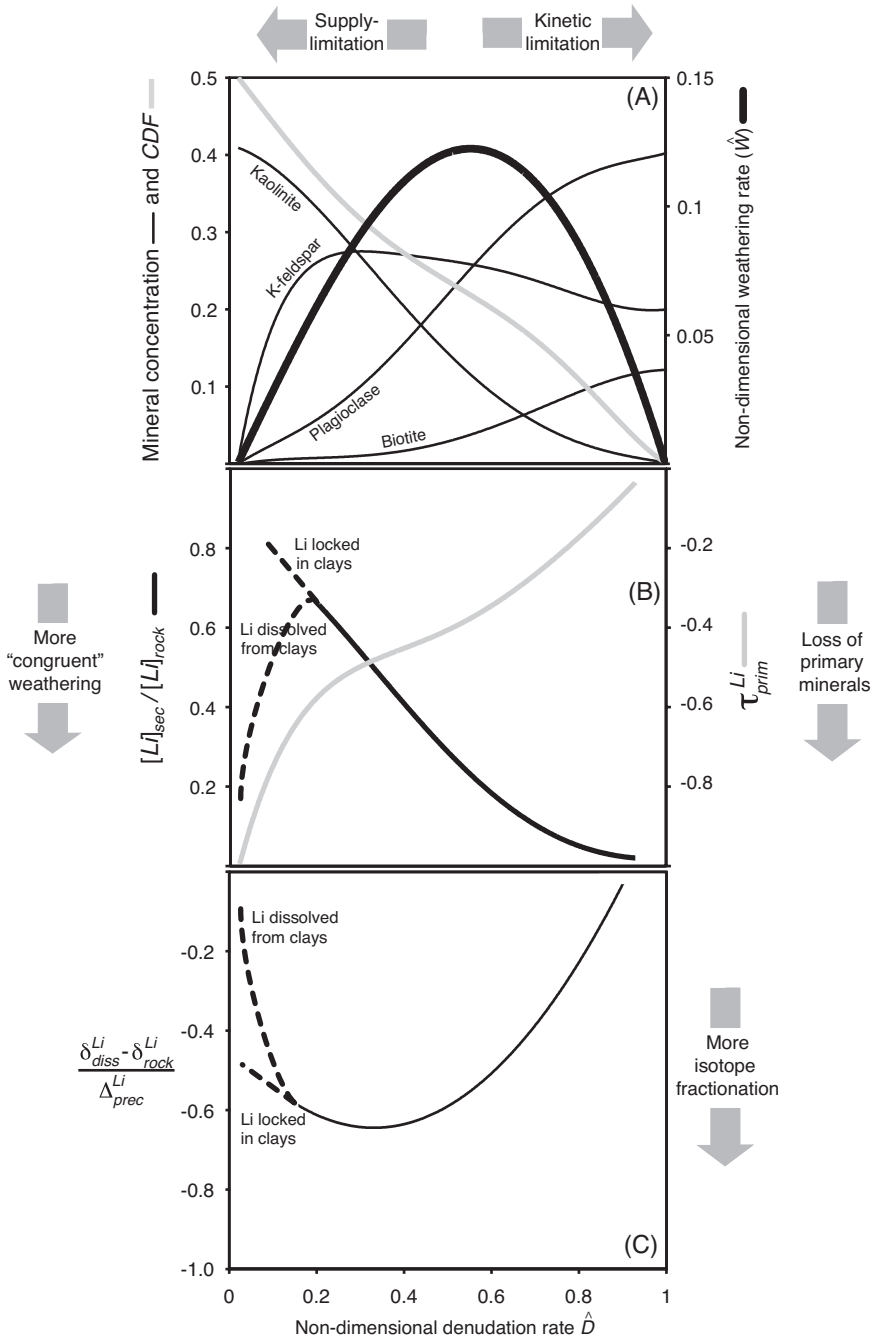

Fig. 9. Modeling of Li behavior in the global weathering zone following the results of Ferrier and Kirchner (2008) (panel A). The bedrock has a granitic composition (quartz is not shown). Non-dimensional denudation rate $\hat{D}$ is the denudation rate D normalized to the maximum soil production rate obtained for an infinitely thin regolith. At high denudation rates, regolith residence time is short and weathering intensities (as shown by *CDF*) and rates (non-dimensional weathering rate $\hat{W}$ that is W normalized to the maximum soil production rate) are low: the system is *kinetically-limited*. At low denudation rates, regolith residence time is long and weathering intensities are high: *CDF* reaches a value of 0.5, and weathering of biotite, plagioclase and K-feldspar run to completion, whereas the maximum amount of precipitated kaolinite is reached.

West and others, 2005; Gabet and Mudd, 2009; Dixon and von Blanckenburg, 2012). Such regimes are characteristic of tectonically quiescent regions such as Central Africa, for example. At the other end of the spectrum, in the "kinetically-limited" regime (West and others, 2005), denudation is high and regolith residence time is so short that minerals do not weather to completion before the solid material is eroded, and the weathering fluxes are limited by dissolution kinetics. This regime is expected to be encountered in high-standing collisional orogens or oceanic islands.

Ferrier and Kirchner (2008) and Gabet and Mudd (2009) have parameterized the different geomorphic regimes at steady-state as a function of denudation rates, and predicted the associated weathering rates. In these models, the relationship between soil residence time and supply of minerals to the weathering zone is described by the so-called "soil production function" (Heimsath and others, 1997). This relationship shows that regolith thickness, and hence residence time, decreases with increasing regolith production rate. We use the model of Ferrier and Kirchner (2008) to predict the steady-state concentration of minerals (quartz, plagioclase, K-feldspar, biotite, kaolinite) in a regolith developed over a granitic rock as a function of erosion or denudation rate and we apply this model to the partitioning of Li under weathering conditions at the global scale. The following assumptions are made: (1) in unweathered granite, Li is hosted only by biotite and K-feldspar, and in equal proportions; (2) secondary precipitate-hosted Li is calculated assuming kaolinite as the only host; (3) Li is incorporated into secondary weathering products at a concentration of 100 ppm (as reported for the highest Li content in shales, and close to the 120 ppm Li reported for smectite formed at 25 °C; Teng and others, 2004; Vigier and others, 2008); (4) Li concentration in unweathered granite is 50 ppm. The results are shown in figure 9.

For moderate denudation rates (that is between 0.2 and 0.8 times the maximum regolith production rate), as denudation rate increases, regolith residence time shortens and more K-feldspar and biotite remain unweathered in topsoil. Also, less kaolinite and other secondary precipitates are formed. At high denudation rates this translates into (1) lower $[Li]_{sec}/[Li]_{rock}$; (2) higher (that is closer to 0, or less negative) values of τ^{X}_{prim} as less Li is unlocked from primary minerals; (3) lower *CDF* as less mass is weathered out of the regolith profile (Ferrier and Kirchner, 2008). The combination of these three effects means that, as the denudation rate increases, less clay is formed and the dissolved Li isotope composition becomes closer to that of rock (fig. 9). However, the dissolution of Li-bearing secondary weathering products is not accounted for by this model. At very low denudation rate, it is expected that the Li contained in secondary precipitates will also be dissolved. In this limiting case, all Li is exported as dissolved species, and $\delta^{Li}_{diss} = \delta^{Li}_{rock}$. This is why a reversal should appear in the denudation regime-water isotope composition relationship (fig. 9C). This means that for a given water isotope composition, there is not a unique denudation rate that

Fig. 9 (continued). However, in this case weathering rates are low as well because unweathered minerals are delivered only slowly into the weathering zone: the system is *supply-limited*. Middle panel (B): model of the budget required to predict Li isotope ratios in waters by equation (16). $[Li]_{sec}/[Li]_{rock}$ decreases with increasing denudation rate as regolith residence time decreases and as secondary minerals have less time to form and incorporate Li. Here kaolinite is assumed to be representative of all secondary weathering products incorporating Li, and Li is assumed to be incorporated at a concentration of 120 ppm in these minerals (Vigier and others, 2008). At very low denudation rate, it is expected that Li is leached from secondary precipitates as well, a process that is not accounted for by Ferrier and Kirchner (2008)'s model. The stippled trend "Li locked in clays" reflect the direct results from Ferrier and Kirchner (2008)'s model, whereas the stippled curved trend "Li dissolved from clays" reflects a rough estimate of the expected trend if Li from clays is leached. $[Li]_{rock}$ is assumed to be 100 ppm throughout. τ^{X}_{prim} is the fractional loss of Li from primary minerals, which is highest (tending towards −1) at low denudation rate, when soil residence time is long enough so that biotite and K-feldpar hosting Li are weathered. Bottom panel: prediction of the normalized difference between the Li isotope composition of river water and of the upper continental crust using *CDF*, $[Li]_{sec}/[Li]_{rock}$ and τ^{X}_{prim}, following equation (16). Stippled lines are as in the middle panel.

can be inferred, as the relationship between denudation rate and isotope composition is not monotonous. Another result is emerging when clay dissolution is considered. Then the largest absolute value of $(\delta^{Li}_{diss} - \delta^{Li}_{rock})/\bar{\Delta}^{Li}_{prec}$ is not 1 (fig. 9). Finally, it should be emphasized that at high denudation rate, a large uncertainty is carried by Ferrier and Kirchner (2008)'s model, since in this case the fluxes of Li dissolved from primary minerals and precipitated in secondary weathering products are both very small.

Although establishing the exact curve relating $(\delta^{Li}_{diss} - \delta^{Li}_{rock})/\bar{\Delta}^{Li}_{prec}$ with denudation rate would require further research pertaining to the elemental behavior of Li during weathering as a function of geomorphic regime, this analysis shows that two situations can lead to $(\delta^{Li}_{diss} - \delta^{Li}_{rock}) = 0$, regardless of the isotope fractionation factor:

(1) If the denudation rate is very low and the global weathering system is supply-limited. In this scenario, all Li is leached from minerals, even from secondary weathering products, before being exported to the oceans.

(2) If the denudation rate is very high, that is at the maximum soil production rate. In this case, a fraction of source-rock Li simply remains unlocked from primary minerals, and is not incorporated into secondary weathering products before being exported to the oceans.

Both these scenarios correspond to "congruent weathering" of Li, meaning that no export of Li as isotopically-fractionated solid material such as clays or oxides takes place. Hence, the early Cenozoic oceanic Li isotope data (Misra and Froelich, 2012) can be interpreted as reflecting either of these two diametrically opposed geomorphic regimes. However, from geologic considerations we see no evidence that denudation rates and soil production rates should have been higher in the early Cenozoic than today. Hence, the variation of δ^{Li}_{diss} throughout the Cenozoic (fig. 7) most likely indicates that the Earth's global weathering system shifted indeed from an extremely low denudation regime to a more intermediate geomorphic regime, where the effect of Li isotope fractionation became more pronounced (fig. 9). According to the Li isotope curve (fig. 8), the Earth surface has resided in this intermediate regime for the last 6 Myrs.

CONCLUSIONS

We provide the first quantitative framework bridging approaches from the fields of geomorphology and novel isotope geochemistry in the compartments of the weathering zone. The model we developed (1) is solely based on a steady-state mass balance for element fluxes and isotope ratios and does not rely on any parameterization of the underlying mechanisms; (2) applies to any novel stable isotope system; (3) considers that only formation of secondary weathering products and uptake by vegetation fractionate isotopes in the weathering zone. The main findings are:

(1) The isotope composition of an element in the compartments of the weathering zone is controlled by the combination of (a) the rate of release of this element to water through primary mineral dissolution; (b) the erosion rate of this element as isotopically fractionated material, that is as secondary precipitates and solid organic matter; (c) the associated isotope fractionation factors. More specifically, the isotope composition of dissolved species in water will evolve away from that of source rock if the ratio of (a) to (b) is high. The effect of (c) is best represented by a "lumped" isotope fractionation factor that is a weighted average of the isotope fractionation factors associated with secondary mineral precipitation and uptake of this element by plants.

(2) Isotope ratios measured in the weathering zone compartments can now be linked to isotope fractionation factors through either (a) element fluxes into and from the weathering zone, and between compartments; or (b) chemical weathering indexes measured on regolith material; or (c) element concentrations measured in compartments of the weathering zone or on river dissolved and particulate material. Our

approach provides a means to calibrate isotope fractionation factors from measurements on field material. It is essential, however, that isotope ratios and chemical concentrations are measured on separates from regolith or river sediment, such as secondary precipitates, organic material, and primary minerals, and not only on bulk material.

(3) If the isotope composition of an element is known in the dissolved form, in particulate material, and in bedrock, the solid-to-dissolved export ratio of this element can be inferred.

(4) If an element is preserved in the sedimentary record, its stable isotopes can be quantitatively interpreted in terms of past relative fluxes into, within and from the weathering zone, or in terms of changes in isotope fractionation factors.

(5) The geomorphic regime controls isotope ratios in the compartments of the weathering zone through the interplay between regolith residence time and kinetics of mineral dissolution and precipitation, and organic matter decomposition. From our detailed analysis of these relationships using Li as an example, we tentatively suggest that for any element, the isotope composition of dissolved species in soil or river water exhibits the strongest isotope signature at a "critical" denudation rate. Knowing this critical denudation rate is a prerequisite to reconstruct past geomorphic regimes.

Our model allows for the quantitative interpretation of data on novel isotope systems in weathering systems, but also provides guidelines for sampling strategies for future research in this field. In combination with this model, geomorphological and isotopic approaches will undoubtedly disclose the processes and feedbacks maintaining soils at the Earth surface, while the study of the sedimentary record will unravel their variations through the past.

ACKNOWLEDGMENTS

We are grateful to Marcus Oelze, Mathieu Dellinger, and Jérôme Gaillardet for stimulating and helpful discussions. The manuscript benefited from the insightful comments from Damien Lemarchand, Mike J. Bickle and Philip A. E. Pogge von Strandmann.

Appendix A

Solution of the system of mass-balance equations

Our goal is to predict the isotope composition of solid regolith compartments (δ^X_{prim}, δ^X_{sec}, δ^X_{org}), soil water (δ^X_{diss}), and vegetation (δ^X_{veg}). Combining equations (3a) and (4a), it can be shown that the isotope composition of the regolith primary minerals is the same as that of bedrock (eq 5a):

$$\delta^X_{prim} = \delta^X_{rock} \tag{A1}$$

which derives from the model assumption that no isotope fractionation occurs during delivery of primary minerals from bedrock to regolith, nor during primary mineral dissolution within the regolith. It is then convenient to express δ^X_{sec}, δ^X_{org}, and δ^X_{veg} as a function of δ^X_{diss}. Combining equations (3b) and (4b), one obtains equation (5b):

$$\delta^X_{sec} = \delta^X_{diss} + \Delta^X_{prec}. \tag{A2}$$

Using equations (3d) and (4d), the isotopic composition of the plant compartment can be calculated (eq 5d):

$$\delta^X_{veg} = \delta^X_{diss} + \Delta^X_{upt}. \tag{A3}$$

Combining equations (3c) and (4c), one can show that the isotope composition of the solid organic matter is at steady-state equal to that of the vegetation compartment, yielding equation (5c):

$$\delta^X_{org} = \delta^X_{veg} = \delta^X_{diss} + \Delta^X_{upt}. \tag{A4}$$

Now δ^X_{diss} has to be determined. If the bedrock isotope composition δ^X_{rock} is assumed to be fixed, the relevant parameter to express is $(\delta^X_{diss} - \delta^X_{rock})$. Substitution of equations (A1), (A3), and (A4) into equation (4e):

$$(S^X_{rock} + S^X_{prim}) \cdot \delta^X_{rock} + S^X_{sec} \cdot (\delta^X_{diss} + \Delta^X_{prec}) + S^X_{org} \cdot (\delta^X_{diss} + \Delta^X_{upt}) = P^X \cdot (\delta^X_{diss} + \Delta^X_{prec}) + U^X \cdot (\delta^X_{diss} + \Delta^X_{upt}) + W^X \cdot \delta^X_{diss} \tag{A5}$$

which is equivalent to the following equation, obtained by simple rearrangement:

$$(S^X_{rock} + S^X_{prim}) \cdot \delta^X_{rock} + (S^X_{sec} + S^X_{org} - P^X - U^X - W^X) \cdot \delta^X_{diss} = (P^X - S^X_{sec}) \cdot \Delta^X_{prec} + (U^X - S^X_{org}) \cdot \Delta^X_{upt} \tag{A6}$$

which can be converted to (eqs 3b to 3e):

$$(S^X_{rock} + S^X_{prim}) \cdot (\delta^X_{rock} - \delta^X_{diss}) = E^X_{sec} \cdot \Delta^X_{prec} + E^X_{org} \cdot \Delta^X_{upt}. \tag{A7}$$

Rearrangement yields equation (5e):

$$\delta^X_{diss} = \delta^X_{rock} - \frac{E^X_{sec} \cdot \Delta^X_{prec} + E^X_{org} \cdot \Delta^X_{upt}}{S^X_{rock} + S^X_{prim}}. \tag{A8}$$

Appendix B

compilation of dissolved species isotope composition in soil water and river water

A prediction of our steady-state batch reactor is that the difference in isotope ratios $(\delta^X_{diss} - \delta^X_{rock})$ should not be greater than $-\bar{\Delta}^X$. Exceptions from this predicition can only occur if an extreme depletion of a specific isotope along a reactive flowpath takes place by Rayleigh processes. We can tests this hypothesis by comparing measured values of $(\delta^X_{diss} - \delta^X_{rock})$ in natural settings to known isotope fractionation factors. We compiled nearly 1,200 reported isotope composition of dissolved B, Li, Mg, Si, and Ca in soil water, ground water, and river water from about 50 studies (Huh and others, 1998, 2001; Zhu and McDougall, 1998; De La Rocha and others, 2000; Rose and others, 2000; Lemarchand and others, 2002, 2010; Pistiner and Henderson, 2003; Schmitt and others, 2003; Ding and others, 2004, 2011; Kisakürek and others, 2005; Wiegand and others, 2005; Ziegler and others, 2005a, 2005b; Georg and others, 2006, 2007, 2009a, 2009b; Lemarchand and Gaillardet, 2006; Pogge von Strandmann, 2006, 2008, 2010, 2012; Tipper and others, 2006a, 2006b, 2008a, 2010a, 2010b, 2012a, 2012b; Brenot and others, 2008; Jacobson and Holmden, 2008; Cenki-Tok and others, 2009; Chetelat and others, 2009; Vigier and others, 2009; Cardinal and others, 2010; Cividini and others, 2010; Engström and others, 2010; Holmden and Bélanger, 2010; Jacobson and others, 2010; Millot and others, 2010; Négrel and others, 2010; Wimpenny and others, 2010a, 2011; Louvat and others, 2011; Hindshaw and others, 2011; Hughes and others, 2011; Bolou-Bi and others, 2012).

Soil water and river water isotope composition is influenced not only by silicate and carbonate weathering processes, but also by evaporite weathering and by atmospheric (rain, dust) and anthropogenic inputs. First, river data obviously greatly influenced by hydrothermal or anthropogenic inputs were not considered at all for this compilation (for example some of the river data in Lemarchand and others, 2002; Kisakürek and others, 2005; Pogge von Strandmann and others, 2006, 2008, 2010; Louvat and others, 2011). Second, where necessary and possible, the δ^X_{diss} data was corrected, yielding an "external inputs-corrected" dataset (n = 574). Such correction was not applied to soil water and groundwater data, which thus do not feature in the external inputs-corrected dataset except for the soil water data from Pogge von Strandmann and others (2012). In cases where in the original study the atmospheric precipitation input is discussed or estimated using the isotope data (for example Tipper and others, 2010a), no attempt was made to correct the data, which was not included in the external inputs-corrected dataset. For Si isotopes, no correction needs to be applied. Similarly, some authors have checked that the precipitation correction is minute for B, Li, Mg, or Ca isotopes (Huh and others, 2001; Lemarchand and others, 2002; Lemarchand and Gaillardet, 2006; Hindshaw and others, 2011; Millot and others, 2010; Wimpenny and others, 2011; Tipper and others, 2006b, 2010b, 2012a, 2012b). In those cases, the published data was directly used in the external inputs-corrected dataset. Finally, some studies already report external inputs-corrected data (Rose and others, 2000; Chetelat and others, 2009; Pogge von Strandmann and others, 2012). For the other studies, provided that the isotope composition of relevant rain, snow, or throughfall samples is reported, we performed the correction for atmospheric inputs using the fraction of dissolved *X* derived from atmospheric inputs determined by the authors using mixing diagrams or mass balance arguments (Cenki-Tok and others, 2009; Cividini and others, 2010; Lemarchand and others, 2010; Bolou-Bi and others, 2012) or using *X*/Cl

ratios in precipitation and Cl^- concentration in river water (Pogge von Strandmann and others, 2006, 2008, 2010; Louvat and others, 2011). In the latter case, when the correction on *X* concentration was too important (that is more than 50%), the corrected data was not included in the external inputs-corrected dataset.

In many studies, the isotope composition of local rocks are reported and were taken as δ^X_{rock} (Ziegler and others, 2005a, 2005b; Georg and others, 2007; Brenot and others, 2008; Jacobson and Holmden, 2008; Pogge von Strandmann and others, 2008; Tipper and others, 2008a, 2012a; Cividini and others, 2010; Jacobson and others, 2010; Holmden and Bélanger, 2010; Lemarchand and others, 2010; Millot and others, 2010; Wimpenny and others, 2010a; Hindshaw and others, 2011; Bolou-Bi and others, 2012).

At the soil scale and for monolithological catchments, if no rock isotope data is provided (Pistiner and Henderson, 2003; Wiegand and others, 2005; Georg and others, 2006, 2009a; Pogge von Strandmann and others, 2006, 2010, 2012; Tipper and others, 2010a; Cenki-Tok and others, 2009; Vigier and others, 2009; Wimpenny and others, 2011), we used estimates of isotope composition for natural rocks or rock reference materials similar to those underlying the regolith or drained by the rivers (Amini and others, 2009; Schuessler and others, 2009; Li and others, 2010; Pogge von Strandmann and others, 2011). For some studies at the large river scale, isotope composition of different rivers draining different lithologies are reported. This can be problematic for Li (which features a range in isotope composition over 10‰ between basalt, granite and shales) and especially for Mg and Ca as the isotope composition of these two elements differs significantly between silicate and carbonate rocks. For rivers draining monolithological catchments, only the data for the relevant type of rock, when provided, was used (Tipper and others, 2008; also in Brenot and others, 2008). For rivers draining more than one lithology, no attempt was made to estimate δ^{Ca}_{rock} and δ^{Mg}_{rock} except in cases where the isotope composition of river sediment can be used as a proxy for δ^X_{rock} (Millot and others, 2010; Tipper and others, 2012b). For Li in larger rivers (Kisakürek and others, 2005; Huh and others, 2001), we used different estimates of rock isotope composition (Teng and others, 2004, 2009) depending on the catchment lithology. We assumed that the B isotope composition of the continental crust reported by Chaussidon and Albarède is a valid bedrock composition for most studies on B isotope in large rivers (Rose and others, 2000; Lemarchand and others, 2002; Lemarchand and Gaillardet, 2006; Chetelat and others, 2009). Finally, for all studies on Si isotopes at the soil or the small river scale where no isotope composition of local rock is reported (Georg and others, 2006, 2009b; Engström and others, 2010), as well as for studies at the large river scale (De La Rocha and others, 2000; Ding and others, 2004, 2011; Georg and others, 2009a; Cardinal and others, 2010; Hughes and others, 2011), the isotope composition of granites reported by Savage and others (2012) was used.

When necessary, the isotope ratio and isotope fractionation factor data was converted to a common δ-scale across the dataset: $\delta^{7/6}Li_{L\text{-}SVEC}$, $\delta^{11/10}B_{SRM951}$, $\delta^{26/24}Mg_{DSM\text{-}3}$, $\delta^{30/28}Si_{NBS\text{-}28}$, and $\delta^{44/42}Ca_{SRM915a}$. Mg isotope data initially reported on the $\delta^{26/24}Mg_{SRM980}$-scale (for example de Villiers and others, 2005) was not used, since the corresponding reference material has been shown to be heterogeneous (Galy and others, 2003). The probability density functions plotted in figure 2 were obtained by fitting the distribution histograms by a non-parametric kernel smoothing distribution.

Appendix C

Uncertainty propagation for the estimation of the solid-to-dissolved export ratio from isotope composition

Using uncertainty propagation analysis, the uncertainty on a proportion of dissolved export w^X calculated from isotope ratios can be estimated. Following equation (18), w^X is a function of δ^X_{sed}, δ^X_{diss}, and δ^X_{rock}, three mathematically independent variables. The uncertainty on w^X (for example expressed as standard deviation) is called here $\sigma(w^X)$ and will be given by:

$$[\sigma(w^X)]^2 = \left[\left(\frac{\partial w^X}{\partial \delta^X_{sed}}\right)\cdot\sigma(\delta^X_{sed})\right]^2 + \left[\left(\frac{\partial w^X}{\partial \delta^X_{diss}}\right)\cdot\sigma(\delta^X_{diss})\right]^2 + \left[\left(\frac{\partial w^X}{\partial \delta^X_{rock}}\right)\cdot\sigma(\delta^X_{rock})\right]^2 \quad \text{(C1)}$$

where $\sigma(\delta^X_{sed})$, $\sigma(\delta^X_{diss})$, and $\sigma(\delta^X_{rock})$ are the uncertainties on the topsoil/sediment, soil water/river water and rock isotope composition, respectively. Calculating the partial derivatives, equation (C1) becomes:

$$[\sigma(w^X)]^2 = \left[\left(\frac{1-w^X}{\delta^X_{sed}-\delta^X_{diss}}\right)\cdot\sigma(\delta^X_{sed})\right]^2 + \left[\left(\frac{w^X}{\delta^X_{sed}-\delta^X_{diss}}\right)\cdot\sigma(\delta^X_{diss})\right]^2 + \left[\left(\frac{1}{\delta^X_{sed}-\delta^X_{diss}}\right)\cdot\sigma(\delta^X_{rock})\right]^2. \quad \text{(C2)}$$

Defining $\bar{\sigma}(\delta^X_i) = \dfrac{\sigma(\delta^X_i)}{\delta^X_{sed}-\delta^X_{diss}}$ (with $i = sed$, $diss$, or org), equation (C2) reads:

$$[\sigma(w^X)]^2 = [(1 - w^X) \cdot \bar{\sigma}(\delta^X_{sed})]^2 + [w^X \cdot \bar{\sigma}(\delta^X_{diss})]^2 + [\bar{\sigma}(\delta^X_{rock})]^2. \quad \text{(C3)}$$

Equation (C3) shows first that the uncertainty on w^X will be smaller in cases where $(\delta^X_{sed} - \delta^X_{diss})$ is large, that is when fractionation is effective in producing different isotope signatures between the dissolved and particulate loads.

Second, equation (C3) also demonstrates that in low-w^X settings, where most of the export of X is engineered by the sediment, the uncertainty on δ^X_{sed} dominates. This is because in these settings, δ^X_{sed} is close to δ^X_{rock}, yielding a numerator in equation (18) that is close to zero. Such high uncertainties on δ^X_{sed} are likely to be an issue when river sediment is sampled, if a potential grain size-dependence of isotope composition of sediment is not accounted for.

Conversely, the uncertainty on δ^X_{diss} will be dominating in high-w^X settings (that is where the export is dominated by the dissolved load). This is not problematic in terms of the relative uncertainty on w^X, which has a large value (close to 1) in these cases. However, the relative uncertainty on the proportion of particulate export of X is much larger, as this is calculated from $(1 - w^X)$. The uncertainty $\sigma(\delta^X_{diss})$ will be high at the soil scale if there is no means to integrate for the potential variability of soil water composition with depth.

Finally, the uncertainty on δ^X_{rock} contributes to $\sigma(w^X)$ equally for any export regime. Large uncertainties on δ^X_{rock} are likely to characterize small river basins, where representative bedrock is difficult to sample and where the spatial scale is not large enough to average over different rock types as is possible at the large river scale.

The uncertainty on w^X can be traced as a function of w^X if values for $\bar{\sigma}(\delta^X_i)$ are assumed. In the following we focus on the small river scale but assume for simplicity that the bedrock isotope composition is known with the highest precision ($\bar{\sigma}(\delta^X_{rock}) = 0$). However, including an uncertainty on δ^X_{rock} would shift $\sigma(w^X)$ towards higher values uniformally across the range of w^X (eq C3). To constrain the values of $\sigma(\delta^X_{sed})$ we use the variability reported Li and Mg isotope compositions between river suspended and bed load in Iceland, Azores and Greenland (Pogge von Strandmann and others, 2006, 2010; Wimpenny and others, 2010b; 2011). From these studies, $\sigma(\delta^{Li}_{sed})$ is in the range 1 to 3‰, while $\sigma(\delta^{Mg}_{sed})$ is around 0.05‰. From the same studies, values of $(\delta^X_{sed} - \delta^X_{diss})$ can be estimated; $(\delta^{Li}_{sed} - \delta^{Li}_{diss})$ is typically 20‰ and $(\delta^{Mg}_{sed} - \delta^{Mg}_{diss})$ is 0.6‰. Hence, for both elements, $\bar{\sigma}(\delta^X_{sed})$ are estimated to be around 0.1. None of these studies report the temporal variability of river dissolved load isotope composition, which potentially is the highest source of uncertainty on δ^X_{diss}. However, Lemarchand and others (2010) reported a time-series of Li isotope composition in the dissolved load of a small river of the Strengbach catchment over 3 years that cover different precipitation regimes. The standard deviation of this dataset is around 2‰ (n = 28), which we take as an estimate of $\sigma(\delta^{Li}_{diss})$. Similarly, we use the standard deviation of dissolved Mg isotope composition reported by Tipper and others (2012b) from a small river draining the Damma Glacier forefield, Swiss Alps, over 6 months (n = 10), yielding a typical value of $\sigma(\delta^{Mg}_{diss}) = 0.05$‰. Therefore, it can be estimated that $\bar{\sigma}(\delta^X_{diss})$ are also around 0.1 for both Mg and Li. These values are used to calculate $\sigma(w^X)$ as a function of w^X in figure 6. No correction for precipitation (rain, snow) was applied here.

Appendix D

Ocean steady-state model for Li concentration and isotopes

Following the approach and the constraints given by Misra and Froelich (2012), we calculate the evolution of river dissolved δ^7Li, called here δ^{Li}_{diss}, from the reported the ocean δ^{Li}_{oc}. We assume quasi steady-state for Li in the ocean at the 1 Myr-timescale, and a negligible Li isotope fractionation for carbonate precipitation from seawater. The two steady-state mass balances for Li mass M^{Li}_{oc} and isotopes are:

$$F^{Li}_{riv} + F^{Li}_{hydr} + F^{Li}_{subd} = F^{Li}_{rev} + F^{Li}_{alt} \quad \text{(D1)}$$

$$F^{Li}_{riv} \cdot \delta^{Li}_{diss} + F^{Li}_{hydr} \cdot \delta^{Li}_{hydr} + (F^{Li}_{subd} - F^{Li}_{rev} - F^{Li}_{alt}) \cdot (\delta^{Li}_{oc} + \Delta^{Li}_{oc\text{-}sed}) = 0 \quad \text{(D2)}$$

where F^{riv}_{Li}, F^{hydr}_{Li} and F^{subd}_{Li} are Li fluxes to the oceans from rivers (dissolved Li only), hydrothermal activity and fluid expulsion at subduction zones. They are assumed to be constant over the Cenozoic (at 10, 13, and $6 \cdot 10^9$ mol yr^{-1}, respectively). F^{Li}_{rev} and F^{Li}_{alt} are oceanic Li sinks by Li incorporation into authigenic clays ("reverse weathering") and by weathering of the oceanic crust (their sum is assumed to be constant and equal to $29 \cdot 10^9$ mol yr^{-1}). δ^{Li}_{hydr} is the Li isotope composition of hydrothermal fluids (constant value of 8.3‰; Misra and Froelich, 2012), and $\Delta^{Li}_{oc\text{-}sed}$ is the isotope fractionation factor related to the sink processes (constant value of −16‰; Misra and Froelich, 2012). Solving these two equations, the Li isotope composition of dissolved Li in rivers is:

$$\delta^{Li}_{diss} = \delta^{Li}_{oc} + \frac{F^{Li}_{hydr}}{F^{Li}_{riv}}(\delta^{Li}_{oc} - \delta^{Li}_{hydr}) + \Delta^{Li}_{oc\text{-}sed} \cdot \left(1 + \frac{F^{Li}_{hydr}}{F^{Li}_{riv}}\right). \quad \text{(D3)}$$

Results are plotted in figure 7. Importantly, Misra and Froelich (2012) have carried out a sensitivity analysis to show that the obtained results for δ^{Li}_{diss} are robust within a large range of values of F^{Li}_{riv}.

References

Amini, M., Eisenhauer, A., Böhm, F., Holmden, C., Kreissig, K., Hauff, F., and Jochum, K. P., 2009, Calcium isotopes ($\delta^{44/40}$Ca) in MPI-DING reference glasses, USGS rock powders and various rocks: Evidence for Ca isotope fractionation in terrestrial silicates: Geostandards and Geoanalytical Research, v. 33, n. 2, p. 231–247, http://dx.doi.org/10.1111/j.1751-908X.2009.00903.x

Anbar, A. D., Jarzecki, A. A., and Spiro, T. G., 2005, Theoretical investigation of iron isotope fractionation between $Fe(H_2O)^{3+}$ and $Fe(H_2O)^{2+}$: Implications for iron stable isotope geochemistry: Geochimica et Cosmochimica Acta, v. 69, n. 4, p. 825–837, http://dx.doi.org/10.1016/j.gca.2004.06.012

Anderson, S. P., von Blanckenburg, F., and White, A. F., 2007, Physical and chemical controls on the Critical Zone: Elements, v. 3, n. 5, p. 315–319, http://dx.doi.org/10.2113/gselements.3.5.315

Bergquist, B. A., and Boyle, E. A., 2006, Iron isotopes in the Amazon River system: Weathering and transport signatures: Earth and Planetary Science Letters, v. 248, n. 1–2, p. 54–68, http://dx.doi.org/10.1016/j.epsl.2006.05.004

Bern, C. R., Brzezinski, M. A., Beucher, C., Ziegler, K., and Chadwick, O. A., 2010, Weathering, dust, and biocycling effects on soil silicon isotope ratios: Geochimica et Cosmochimica Acta, v. 74, p. 876–889, http://dx.doi.org/10.1016/j.gca.2009.10.046

Black, J. R., Epstein, E., Rains, W. D., Yin, Q.-Z., and Casey, W. H., 2008, Magnesium-isotope fractionation during plant growth: Environmental Science & Technology, v. 42, n. 21, p. 7831–7836, http://dx.doi.org/10.1021/es8012722

Bolou-Bi, E., Poszwa, A., Leyval, C., and Vigier, N., 2010, Experimental determination of magnesium isotope fractionation during higher plant growth: Geochimica et Cosmochimica Acta, v. 74, n. 9, p. 2523–2537, http://dx.doi.org/10.1016/j.gca.2010.02.010

Bolou-Bi, E. B., Vigier, N., Poszwa, A., Boudot, J.-P., and Dambrine, E., 2012, Effects of biogeochemical processes on magnesium isotope variations in a forested catchment in the Vosges Mountains (France): Geochimica et Cosmchimica Acta, v. 87, p. 341–355, http://dx.doi.org/10.1016/j.gca.2012.04.005

Bouchez, J., Gaillardet, J., France-Lanord, C., Maurice, L., and Dutra-Maia, P., 2011, Grain size control of river suspended sediment geochemistry: Clues from Amazon River depth profiles: Geochemistry, Geophysics, Geosystems, v. 12, n. 3, GC00380, http://dx.doi.org/10.1029/2010GC003380

Brantley, S. L., and Lebedeva, M., 2011, Learning to read the chemistry of regolith to understand the Critical Zone: Annual Review of Earth and Planetary Sciences, v. 39, p. 387–416, http://dx.doi.org/10.1146/annurev-earth-040809-152321

Brantley, S. L., Liermann, L. J., Guynn, R. L., Anbar, A. D., Icopini, G. A., and Barling, J., 2004, Fe isotopic fractionation during mineral dissolution with and without bacteria: Geochimica et Cosmochimica Acta, v. 68, n. 15, p. 3189–3204, http://dx.doi.org/10.1016/j.gca.2004.01.023

Brantley, S. L., Kubicki, J. D., and White, A. F., 2008, Kinetics of water-rock interaction: New York, Springer, 833 p.

Brantley, S. L., Megonigal, J. P., Scatena, F. N., Balogh Brunstad, Z., Barnes, R. T., Bruns, M. A., van Capellen, P., Dontsova, K., Hartnett, H. E., Hartshorn, A. S., Heimsath, A., Herndon, E., Jin, L., Keller, C. K., Leake, J. R., McDowell, W. H., Meinzer, F. C., Mozder, T. J., Petsch, S., Pett-Ridge, J., Pregitzer, K. S., Ramond, P. A., Riebe, C. S., Shumaker, K., Sutton-Grier, A., Walter, R., and Yoo, K., 2011, Twelve testable hypotheses on the geobiology of weathering: Geobiology, v. 9, n. 2, p. 140–165, http://dx.doi.org/10.1111/j.1472-4669.2010.00264.x

Brenot, A., Cloquet, C., Vigier, N., Carignan, J., and France-Lanord, C., 2008, Magnesium isotope systematics of the lithologically varied Moselle river basin, France: Geochimica et Cosmochimica Acta, v. 72, n. 20, p. 5070–5089, http://dx.doi.org/10.1016/j.gca.2008.07.027

Bullen, T. D., White, A. F., Childs, C. W., Vivit, D. V., and Schulz, M. S., 2001, Demonstration of significant abiotic iron isotope fractionation in nature: Geology, v. 29, n. 8, p. 699–702, http://dx.doi.org/10.1130/0091-7613(2001)029⟨0699:DOSAII⟩2.0.CO;2

Calmels, D., Galy, A., Hovius, N., Bickle, M., West, A. J., Chen, M.-C., and Chapman, H., 2011, Contribution of deep groundwater to the weathering budget in a rapidly eroding mountain belt, Taiwan: Earth and Planetary Science Letters, v. 303, n. 1–2, p. 48–58, http://dx.doi.org/10.1016/j.epsl.2010.12.032

Cardinal, D., Gaillardet, J., Hughes, H. J., Opfergelt, S., and André, L., 2010, Contrasting silicon isotope signatures in rivers from the Congo Basin and the specific behaviour of organic-rich waters: Geophysical Research Letters, v. 37, n. 12, L12403, http://dx.doi.org/10.1029/2010GL043413

Cenki-Tok, B., Chabaux, F., Lemarchand, D., Schmitt, A.-D., Pierret, M.-C., Viville, D., Bagard, M.-L., and Stille, P., 2009, The impact of water-rock interaction and vegetation on calcium isotope fractionation in soil- and stream waters of a small, forested catchment (the Strengbach case): Geochimica et Cosmochimica Acta, v. 73, n. 8, p. 2215–228, http://dx.doi.org/10.1016/j.gca.2009.01.023

Chadwick, O. A., Brimhall, G. H., and Hendricks, D. M., 1990, From a black to a gray box—a mass balance interpretation of pedogenesis: Geomorphology, v. 3, n. 3–4, p. 369–390, http://dx.doi.org/10.1016/0169-555X(90)90012-F

Chan, L. H., Edmond, J. M., Thompson, G., and Gillis, K., 1992, Lithium isotopic composition of submarine

basalts: implications for the lithium cycle in the oceans: Earth and Planetary Science Letters, v. 108, n. 1–3, p. 151–160, http://dx.doi.org/10.1016/0012-821X(92)90067-6
Charlier, B. L. A., Nowell, G. M., Parkinson, I. J., Kelley, S. P., Pearson, D. G., and Burton, K. W., 2012, High temperature strontium stable isotope behaviour in the early solar system and planetary bodies: Earth and Planetary Science Letters, v. 329–330, p. 31–40, http://dx.doi.org/10.1016/j.epsl.2012.02.008
Chetelat, B., Liu, C.-Q., Gaillardet, J., Wang, Q. L., Zhao, Z. Q., Liang, C. S., and Xiao, Y. K., 2009, Boron isotopes geochemistry of the Changjiang basin rivers: Geochimica et Cosmochimica Acta, v. 73, n. 29, p. 6084–6097, http://dx.doi.org/10.1016/j.gca.2009.07.026
Cividini, D., Lemarchand, D., Chabaux, F., Boutin, R., and Pierret, M.-C., 2010, From biological to lithological control of the B geochemical cycle in a forest watershed (Strengbach, Vosges): Geochimica et Cosmochimica Acta, v. 74, n. 11, p. 3143–3163, http://dx.doi.org/10.1016/j.gca.2010.03.002
Cobert, F., Schmitt, A.-D., Bourgeade, P., Labolle, F., Badot, P.-M., Chabaux, F., and Stille, P., 2011, Experimental identification of Ca isotopic fractionations in higher plants: Geochimica et Cosmochimica Acta, v. 75, n. 19, p. 5467–5482, http://dx.doi.org/10.1016/j.gca.2011.06.032
Cornelis, J.-T., Delvaux, B., Cardinal, D., André, L., Ranger, J., and Opfergelt, S., 2010a, Tracing mechanisms controlling the release of dissolved silicon in forest soil solutions using Si isotopes and Ge/Si ratios: Geochimica et Cosmochimica Acta, v. 74, n. 14, p. 3913–3924, http://dx.doi.org/10.1016/j.gca.2010.04.056
Cornelis, J.-T., Delvaux, B., Georg, R. B., Lucas, Y., Ranger, J., and Opfergelt, S., 2011, Tracing the origin of dissolved silicon transferred from various soil-plant systems towards rivers: a review: Biogeosciences Disscussions, v. 8, p. 89–112, http://dx.doi.org/10.5194/bg-8-89-2011
De La Rocha, C. L., and Bickle, M. J., 2005, Sensitivity of silicon isotopes to whole-ocean changes in the silica cycle: Marine Geology, v. 217, n. 3–4, p. 267–282, http://dx.doi.org/10.1016/j.margeo.2004.11.016
De La Rocha, C. L., and DePaolo, D. J., 2000, Isotope evidence for variations in the marine calcium cycle over the Cenozoic: Science, v. 289, n. 5482, p. 1176–1178, http://dx.doi.org/10.1126/science.289.5482.1176
De La Rocha, C. L., Brzezinski, M. A., DeNiro, M. J., and Shemesh, A., 1998, Silicon-isotope composition of diatoms as an indicator of past oceanic change: Nature, v. 395, p. 680–682, http://dx.doi.org/10.1038/27174
De La Rocha, C. L., Brzezinski, M. A., and DeNiro, M. J., 2000, A first look at the distribution of the stable isotopes of silicon in natural waters: Geochimica et Cosmochimica Acta, v. 65, n. 14, p. 2467–2477, http://dx.doi.org/10.1016/S0016-7037(00)00373-2
de Souza, G. F., Reynolds, B. C., Kiczka, M., and Bourdon, B., 2010, Evidence for mass-dependent isotopic fractionation of strontium in a glaciated granitic watershed: Geochimica et Cosmochimica Acta, v. 74, n. 9. p. 2596–2614, http://dx.doi.org/10.1016/j.gca.2010.02.012
de Villiers, S., Dickson, J. A. D., and Ellam, R. M., 2005, The composition of the continental river weathering flux deduced from seawater Mg isotopes: Chemical Geology, v. 216, n. 1–2, p. 133–142, http://dx.doi.org/10.1016/j.chemgeo.2004.11.010
Delstanche, S., Opfergelt, S., Cardinal, D., Elsass, F., André, L., and Delvaux, B., 2009, Silicon isotopic fractionation during adsorption of aqueous monosilicic acid onto iron oxide: Geochimica et Cosmochimica Acta, v. 73, n. 4, p. 923–934, http://dx.doi.org/10.1016/j.gca.2008.11.014
DePaolo, D. J., 2011, Surface kinetic model for isotopic and trace element fractionation during precipitation of calcite from aqueous solutions: Geochimica et Cosmochimica Acta, v. 75, n. 4, p. 1039–1056, http://dx.doi.org/10.1016/j.gca.2010.11.020
Ding, T., Wan, D., Wang, C., and Zhang, F., 2004, Silicon isotope compositions of dissolved silicon and suspended matter in the Yangtze River, China: Geochimica et Cosmochimica Acta, v. 68, n. 2, p. 205–216, http://dx.doi.org/10.1016/S0016-7037(03)00264-3
Ding, T. P., Zhou, J. X., Wan, D. F., Chen, Z. Y., Wang, C. Y., and Zhang, F., 2009, Silicon isotope fractionation in bamboo and its significance to the biogeochemical cycle of silicon: Geochimica et Cosmochimica Acta, v. 72, n. 5, p. 1381–1395, http://dx.doi.org/10.1016/j.gca.2008.01.008
Ding, T. P., Gao, J. F., Tian, S. H., Wang, H. B., and Li, M., 2011, Silicon isotopic composition of dissolved silicon and suspended particulate matter in the Yellow River, China, with implications for the global silicon cycle: Geochimica et Cosmochimica Acta, v. 75, n. 21, p. 6672–6689, http://dx.doi.org/10.1016/j.gca.2011.07.040
Dixon, J. L., and von Blanckenburg, F., 2012, Soils as pacemakers and limiters of global silicate weathering: Comptes-Rendus Géoscience, v. 344, n. 11–12, p. 597–609, http://dx.doi.org/10.1016/j.crte.2012.10.012
Dixon, J. L., Heimsath, A. M., Kaste, J., and Amundson, R., 2009, Climate-driven processes of hillslope weathering: Geology, v. 37, n. 11, p. 975–978, http://dx.doi.org/10.1130/G30045A.1
dos Santos Pinheiro, G. M., Poitrason, F., Sondag, F., Cruz Vieira, L., and Pimentel, M. M., 2013, Iron isotope composition of the suspended matter along depth and lateral profiles in the Amazon River and its tributaries: Journal of South American Earth Sciences, v. 44, p. 35–44, http://dx.doi.org/10.1016/j.jsames.2012.08.001
Dupré, B., Dessert, C., Oliva, P., Goddéris, Y., Viers, J., François, L., Millot, R., and Gaillardet, J., 2003, Rivers, chemical weathering and Earth's climate: Comptes Rendus Géoscience, v. 335, n. 16, p. 1141–1160, http://dx.doi.org/10.1016/j.crte.2003.09.015
Emmanuel, S., Erel, Y., Matthews, A., and Teutsch, N., 2005, A preliminary mixing model for Fe isotopes in soils: Chemical Geology, v. 222, n. 1–2, p. 23–34, http://dx.doi.org/10.1016/j.chemgeo.2005.07.002
Engström, E., Rodushkin, I., Ingri, J., Baxter, D. C., Ecke, F., Österlund, H., and Öhlander, B., 2010, Temporal variations of dissolved silicon in a pristine boreal river: Chemical Geology, v. 271, n. 3–4, p. 142–152, http://dx.doi.org/10.1016/j.chemgeo.2010.01.005
Ewing, S. A., Yang, W., DePaolo, D. J., Michalski, G., Kendall, C., Stewart, B. W., Thiemens, M., and Amundson, R., 2008, Non-biological fractionation of stable Ca isotopes in soils of the Atacama desert,

Chile: Geochimica et Cosmochimica Acta, v. 72, n. 4, p. 1096–1110, http://dx.doi.org/10.1016/j.gca.2007.10.029
Fantle, M. S., 2010, Evaluating the Ca isotope proxy: American Journal of Science, v. 310, n. 3, p. 194–230, http://dx.doi.org/10.2475/03.2010.03
Fantle, M. S., and DePaolo, D. J., 2004, Iron isotopic fractionation during continental weathering: Earth and Planetary Science Letters, v. 228, n. 3–4, p. 547–562, http://dx.doi.org/10.1016/j.epsl.2004.10.013
——— 2005, Variations in the marine Ca cycle over the past 20 million years: Earth and Planetary Science Letters, v. 237, n. 1–2, p. 102–117, http://dx.doi.org/10.1016/j.epsl.2005.06.024
Ferrier, K. L., and Kirchner, J. W., 2008, Effects of physical erosion on chemical denudation rates: A numerical modeling study of soil-mantled hillslopes: Earth and Planetary Science Letters, v. 272, n. 3–4, p. 591–599, http://dx.doi.org/10.1016/j.epsl.2008.05.024
Ferrier, K. L., Kirchner, J. W., Riebe, C. S., and Finkel, R. C., 2010, Mineral-specific chemical weathering rates over millenial timescales: Measurements at Rio Icacos, Puerto Rico: Chemical Geology, v. 277, n. 1–2, p. 101–114, http://dx.doi.org/10.1016/j.chemgeo.2010.07.013
Fletcher, R. C., Buss, H. L., and Brantley, S. L., 2006, A spheroidal weathering model coupling porewater chemistry to soil thickness during steady-state denudation: Earth and Planetary Science Letters, v. 244, n. 1–2, p. 444–457, http://dx.doi.org/10.1016/j.epsl.2006.01.055
Gabet, E. J., and Mudd, S. M., 2009, A theoretical model coupling chemical weathering rates with denudation rates: Geology, v. 37, n. 2, p. 151–154, http://dx.doi.org/10.1130/G25270A.1
Gaillardet, J., Dupré, B., Louvat, P., and Allègre, C. J., 1999, Global silicate weathering and CO_2 consumption rates deduced from the chemistry of large rivers: Chemical Geology, v. 159, n. 1–4, p. 3–30, http://dx.doi.org/10.1016/S0009-2541(99)00031-5
Gaillardet, J., Viers, J., and Dupré, B., 2003, Trace elements in river waters, *in* Drever, J. I., editor, Surface and Ground Water: Treatise on Geochemistry, v. 5, ch. 9, p. 225–272, http://dx.doi.org/10.1016/B0-08-043751-6/05165-3
Galy, A., Yoffe, O., Janney, P. E., Williams, R. W., Cloqiet, C., Alard, O., Halicz, L., Wadhwa, M., Hutcheon, I. D., Ramon, E., and Carignan, J., 2003, Magnesium isotope heterogeneity of the isotopic standard SRM980 and new reference materials for magnesium-isotope-ratio measurements: Journal of Analytical Atomic Spectrometry, v. 18, n. 11, p. 1352–1356, http://dx.doi.org/10.1039/b309273a
Georg, R. B., Reynolds, B. C., Frank, M., and Halliday, A. N., 2006, Mechanisms controlling the silicon isotopic compositions of river waters: Earth and Planetary Science Letters, v. 249, n. 3–4, p. 290–306, http://dx.doi.org/10.1016/j.epsl.2006.07.006
Georg, R. B., Reynolds, B. C., West, A. J., Burton, K. W., and Halliday, A. N., 2007, Silicon isotope variations accompanying basalt weathering in Iceland: Earth and Planetary Science Letters, v. 261, n. 3–4, p. 476–490, http://dx.doi.org/10.1016/j.epsl.2007.07.004
Georg, R. B., West, A. J., Basu, A. R., and Halliday, A. N., 2009a, Silicon fluxes and isotope composition of direct groundwater discharge into the Bay of Bengal and the effect on the global ocean silicon isotope budget: Earth and Planetary Science Letters, v. 283, n. 1–4, p. 67–74, http://dx.doi.org/10.1016/j.epsl.2009.03.041
Georg, R. B., Zhu, C., Reynolds, B. C., and Halliday, A. N., 2009b, Stable silicon isotopes of groundwater, feldspars, and clay coatings in the Navajo sandstone aquifer, Black Mesa, Arizona, USA: Geochimica et Cosmochimica Acta, v. 73, n. 8, p. 2229–2241, http://dx.doi.org/10.1016/j.gca.2009.02.005
Goudie, A. S., and Viles, H. A., 2012, Weathering and the global carbon cycle: Geomorphological perspectives: Earth Science Reviews, v. 113, n. 1–2, p. 59–71, http://dx.doi.org/10.1016/j.earscirev.2012.03.005
Guelke, M., and von Blanckenburg, F., 2007, Fractionation of stable iron isotopes in higher plants: Environmental Science & Technology, v. 41, n. 6, p. 1896–1901, http://dx.doi.org/10.1021/es062288j
Guelke, M., von Blanckenburg, F., Schoenberg, R., Staubwasser, M., and Stuetzel, H., 2010, Determining the stable Fe isotope signature of plant-available iron in soils: Chemical Geology, v. 277, n. 3–4, p. 269–280, http://dx.doi.org/10.1016/j.chemgeo.2010.08.010
Halliday, A. N., Lee, D.-C., Christensen, J. N., Rehkämper, M., Yi, W., Luo, X., Hall, C. M., Ballentine, C. J., Pettke, T., and Stirling, C., 1998, Applications of multiple collector-ICPMS to cosmochemistry, geochemistry and paleoceanography: Geochimica et Cosmochimica Acta, v. 62, n. 6, p. 919–940, http://dx.doi.org/10.1016/S0016-7037(98)00057-X
Handler, M. R., Baker, J. A., Schiller, M., Bennett, V. C., and Yaxley, G. M, 2009, Magnesium stable isotope composition of Earth's upper mantle: Earth and Planetary Science Letters, v. 282, p. 306–313, http://dx.doi.org/10.1016/j.epsl.2009.03.031
Hathorne, E. C., and James, R. H., 2006, Temporal record of lithium in seawater: a tracer for silicate weathering: Earth and Planetary Science Letters, v. 246, n. 3–4, p. 393–406, http://dx.doi.org/10.1016/j.epsl.2006.04.020
Heimsath, A. M., Dietrich, W. E., Nishiizumi, K., and Finkel, R. C., 1997, The soil production function and landscape equilibrium: Nature, v. 388, p. 358–361, http://dx.doi.org/10.1038/41056
Hindshaw, R. S., Reynolds, B. C., Wiederhold, J. G., Kretzschmar, R., and Bourdon, B., 2011, Calcium isotopes in a proglacial weathering environment: Damma glacier, Switzerland: Geochimica et Cosmochimica Acta, v. 75, n. 1, p. 106–118, http://dx.doi.org/10.1016/j.gca.2010.09.038
Holmden, C., and Bélanger, N., 2010, Ca isotopes cycling in a forested ecosystem: Geochimica et Cosmochimica Acta, v. 74, n. 3, p. 995–1015, http://dx.doi.org/10.1016/j.gca.2009.10.020
Huang, K.-J., Teng, F.-Z., Wei, G.-J., Ma, J.-L., and Bao, Z.-Y., 2012, Adsorption- and desorption-controlled magnesium isotope fractionation during extreme weathering of basalt in Hainan Island, China: Earth and Planetary Science Letters, v. 359–360, p. 73–83, http://dx.doi.org/10.1016/j.epsl.2012.10.007
Hughes, H. J., Sondag, F., Cocquyt, C., Laraque, A., Pandi, A., André, L., and Cardinal, D., 2011, Effect of

seasonal biogenic silica variations on dissolved silicon fluxes and isotopic signatures in the Congo River: Limnology and Oceanography, v. 56, n. 2, p. 551–561, http://dx.doi.org/10.4319/lo.2011.56.2.0551
Huh, Y., Chan, L.-H., Zhang, L., and Edmond, J. M., 1998, Lithium and its isotopes in major world rivers: implications for weathering and the oceanic budget: Geochimica et Cosmochimica Acta, v. 62, n. 12, p. 2039–2051, http://dx.doi.org/10.1016/S0016-7037(98)00126-4
Huh, Y., Chan, L.-H., and Edmond, J. M., 2001, Lithium isotopes as a probe of weathering processes: Orinoco River: Earth and Planetary Science Letters, v. 194, n. 1–2, p. 189–199, http://dx.doi.org/10.1016/S0012-821X(01)00523-4
Huh, Y., Chan, L.-H., and Chadwick, O. A., 2004, Behavior of lithium and its isotopes during weathering of Hawaiian basalt: Geochemistry Geophysics Geosystems, v. 5, n. 9, GC000729, http://dx.doi.org/10.1029/2004GC000729
Ilina, S. M., Poitrasson, F., Lapitskiy, S. A., Alekhin, Y. V., Viers, J., and Pokrovsky, O. S., 2013, Extreme iron isotope fractionation between colloids and particles of boreal and temperate organic-rich waters: Geochimica et Cosmochimica Acta, v. 101, p. 96–111, http://dx.doi.org/10.1016/j.gca.2012.10.023
Ingri, J., Malinovsky, D., Rodushkin, I., Baxter, D. C., Widelund, A., Andersson, P., Gustafsson, Ö., Forsling, W., and Öhlander, B., 2006, Iron isotope fractionation in river colloidal matter: Earth and Planetary Science Letters, v. 245, n. 3–4, p. 792–798, http://dx.doi.org/10.1016/j.epsl.2006.03.031
Jacobson, A. D., and Holmden, C., 2008, δ^{44}Ca evolution in a carbonate aquifer and its bearing on the equilibrium isotope fractionation factor for calcite: Earth and Planetary Science Letters, v. 270, n. 3–4, p. 349–353, http://dx.doi.org/10.1016/j.epsl.2008.03.039
Jacobson, A. D., Zhang, Z., Lundstrom, C., and Huang, F., 2010, Behavior of Mg isotopes during dedolomitization in the Madison Aquifer, South Dakota: Earth and Planetary Science Letters, v. 297, n. 3–4, p. 446–452, http://dx.doi.org/10.1016/j.epsl.2010.06.038
Johnson, C. M., Roden, E. E., Welch, S. A., and Beard, B. L., 2005, Experimental constraints on Fe isotope fractionation during magnetite and Fe carbonate formation coupled to dissimilatory hydrous ferric oxide reduction: Geochimica et Cosmochimica Acta, v. 69, n. 4, p. 963–993, http://dx.doi.org/10.1016/j.gca.2004.06.043
Kiczka, M., Wiederhold, J. G., Frommer, J., Kraemer, S. M., Bourdon, B., and Kretzschmar, R., 2010, Iron isotope fractionation during proton- and ligand-promoted dissolution of primary phyllosilicates: Geochimica et Cosmochimica Acta, v. 74, n. 11, p. 3112–3128, http://dx.doi.org/10.1016/j.gca.2010.02.018
Kiczka, M., Wiederhold, J. G., Frommer, J., Voegelin, A., Kraemer, S. M., Bourdon, B., and Kretzschmar, R., 2011, Iron speciation and isotope fractionation during silicate weathering and soil formation in an alpine glacier forefield chronosequence: Geochimica et Cosmochimica Acta, v. 75, n. 19, p. 5559–5573, http://dx.doi.org/10.1016/j.gca.2011.07.008
Kisakürek, B., Widdowson, M., and James, R. H., 2004, Behaviour of Li isotopes during continental weathering: the Bidar laterite profile, India: Chemical Geology, v. 212, n. 1–2, p. 27–44, http://dx.doi.org/10.1016/j.chemgeo.2004.08.027
Kisakürek, B., James, R. H., and Harris, N. B. W., 2005, Li and δ^{7}Li in Himalayan rivers: Proxies for silicate weathering?: Earth and Planetary Science Letters, v. 237, n. 3–4, p. 387–401, http://dx.doi.org/10.1016/j.epsl.2005.07.019
Klochko, K., Kaufman, A. J., Yao, W., Byrne, R. H., and Tossell, J. A., 2006, Experimental measurement of boron isotope fractionation in seawater: Earth and Planetary Science Letters, v. 248, n. 1–2, p. 276–285, http://dx.doi.org/10.1016/j.epsl.2006.05.034
Lebedeva, M. I., Fletcher, R. C., Balashov, V. N., and Brantley, S. L., 2007, A reactive diffusion model describing transformation of bedrock to saprolite: Chemical Geology, v. 244, n. 3–4, p. 624–645, http://dx.doi.org/10.1016/j.chemgeo.2007.07.008
Lemarchand, D., and Gaillardet, J., 2006, Transient features of the erosion of shales in the Mackenzie basin (Canada), evidences from boron isotopes: Earth and Planetary Science Letters, v. 245, n. 1–2, p. 174–189, http://dx.doi.org/10.1016/j.epsl.2006.01.056
Lemarchand, D., Gaillardet, J., Lewin, É., and Allègre, C. J., 2000, The influence of rivers on marine boron isotopes and implications for reconstructing past ocean pH: Nature, v. 408, p. 951–954, http://dx.doi.org/10.1038/35050058
——— 2002, Boron isotope systematics in large rivers: Implications for the marine boron budget and paleo-pH reconstruction over the Cenozoic: Chemical Geology, v. 190, n. 1–4, p. 123–140, http://dx.doi.org/10.1016/S0009-2541(02)00114-6
Lemarchand, D., Cividini, D., Turpault, M.-P., and Chabaux, F., 2012, Boron isotopes in different grain size fractions: exploring past and present water-rock interactions from two soil profiles (Strengbach, Vosges Mountains): Geochimica et Cosmochimica Acta, v. 98, p. 78–93, http://dx.doi.org/10.1016/j.gca.2012.09.009
Lemarchand, E., Schott, J., and Gaillardet, J., 2005, Boron isotopic fractionation related to boron sorption on humic acid and the structure of the surface complexes formed: Geochimica et Cosmochimica Acta, v. 69, n. 14, p. 3519–3533, http://dx.doi.org/10.1016/j.gca.2005.02.024
——— 2007, How surface complexes impact boron isotope fractionation: Evidence from Fe and Mn oxides sorption experiments: Earth and Planetary Science Letters, v. 260, n. 1–2, p. 277–296, http://dx.doi.org/10.1016/j.epsl.2007.05.039
Lemarchand, E., Chabaux, F., Vigier, N., Millot, R., and Pierret, M.-C., 2010, Lithium isotope systematics in a forested granitic catchment (Strengbach, Vosges Mountains, France): Geochimica et Cosmochimica Acta, v. 74, n. 16, p. 4612–4628, http://dx.doi.org/10.1016/j.gca.2010.04.057
Li, W.-Y., Teng, F.-Z., Ke, S., Rudnick, R. L., Gao, S., Wu, F.-Y., Chappell, B. W., 2010, Heterogeneous magnesium isotopic composition of the upper continental crust: Geochimica et Cosmochimica Acta, v. 74, n. 23, p. 6867–6884, http://dx.doi.org/10.1016/j.gca.2010.08.030

Louvat, P., Gaillardet, J., Paris, G., and Dessert, C., 2011, Boron isotope ratios of surface waters in Guadeloupe, Lesser Antilles: Applied Geochemistry, v. 26, Supplement, p. S76–S79, http://dx.doi.org/10.1016/j.apgeochem.2011.03.035

Lundstrom, C. C., Chaussidon, M., Hsui, A. T., Kelemen, P., and Zimmerman, M., 2005, Observation of Li isotopic variation in the Trinity ophiolite: evidence for isotopic fractionation by diffusion during mantle melting: Geochimica et Cosmochimica Acta, v. 69, n. 3, p. 735–751, http://dx.doi.org/10.1016/j.gca.2004.08.004

Maher, R., 2010, The dependence of chemical weathering rates on fluid residence time: Earth and Planetary Science Letters, v. 294, n. 1–2, p. 101–110, http://dx.doi/org/10.1016/j.epsl.2010.03.010

Marriott, C. S., Henderson, G. M., Belshaw, N. S., and Tudhope, A. W., 2004, Temperature dependence of δ^7Li,δ^{44}Ca and Li/Ca during growth of calcium carbonate: Earth and Planetary Science Letters, v. 222, n. 2, p. 615–624, http://dx.doi.org/10.1016/j.epsl.2004.02.031

Martin, J.-M., and Meybeck, M., 1979, Elemental mass-balance of material carried by major world rivers: Marine Chemistry, v. 7, n. 3, p. 173–206, http://dx.doi.org/10.1016/0304-4203(79)90039-2

Millot, R., Vigier, N., and Gaillardet, J., 2010, Behaviour of lithium and its isotopes during weathering in the Mackenzie Basin, Canada: Geochimica et Cosmochimica Acta, v. 74, n. 14, p. 3897–3912, http://dx.doi.org/10.1016/j.gca.2010.04.025

Misra, S., and Froelich, P. N., 2012, Lithium isotope history of Cenozoic seawater: Changes in silicate weathering and reverse weathering: Science, v. 335, n. 6070, p. 818–823, http://dx.doi.org/10.1126/science.1214697

Négrel, P., Millot, R., Brenot, A., and Bertin, C., 2010, Lithium isotopes as tracers of groundwater circulation in a peat land: Chemical Geology, v. 276, n. 1–2, p. 119–127, http://dx.doi.org/10.1016/j.chemgeo.2010.06.008

Négrel, P., Millot, R., Guerrot, C., Petelet-Giraud, E., Brenot, A., and Malcuit, E., 2012, Heterogeneities and interconnections in groundwaters: Coupled B, Li and stable-isotope variations in a large aquifer system (Eocene Sand aquifer, Southwestern France): Chemical Geology, v. 296–297, p. 83–95, http://dx.doi.org/10.1016/j.chemgeo.2011.12.022

Ockert, C., Gussone, N., Kaufhold, S., and Teichert, B. M. A., 2013, Isotope fractionation of Ca during exchange on clay minerals in a marine environment: Geochimica et Cosmochimica Acta, http://dx.doi.org/10.1016/j.gca.2012.09.041

Opfergelt, S., de Bournonville, G., Cardinal, D., André, L., Delstanche, S., and Delvaux, B., 2009, Impact of soil weathering degree on silicon isotopic fractionation during adsorption onto iron oxides in basaltic ash soils, Cameroon: Geochimica et Cosmochimica Acta, v. 73, n. 24, p. 7226–7240, http://dx.doi.org/10.1016/j.gca.2009.09.003

Opfergelt, S., Cardinal, D., André, L., Delvigne, C., Bremond, L., and Delvaux, B., 2010, Variations of δ^{30}Si and Ge/Si with weathering and biogenic input in tropical basaltic ash soils under monoculture: Geochimica et Cosmochimica Acta, v. 74, n. 1, p. 225–240, http://dx.doi.org/10.1016/j.gca.2009.09.025

Opfergelt, S., Georg, R. B., Burton, K. W., Guicharnaud, R., Siebert, C., Gíslason, S. R., and Halliday, A. N., 2011, Silicon isotopes in allophane as a proxy for mineral formation in volcanic soils: Applied Geochemistry, v. 26, Supplement, p. S115–S118, http://dx.doi.org/10.1016/j.apgeochem.2011.03.044

Opfergelt, S., Georg, R. B., Delvaux, B., Cabidoche, Y.-M., Burton, K. W., and Halliday, A. N., 2012a, Mechanisms of magnesium isotope fractionation in volcanic soil weathering sequences, Guadeloupe: Earth and Planetary Science Letters, v. 341–344, p. 176–185, http://dx.doi.org/10.1016/j.epsl.2012.06.010

——— 2012b, Silicon isotopes and the tracing of desilication in volcanic soil weathering sequences, Guadeloupe: Chemical Geology, v. 326–327, p. 113–122, http://dx.doi.org/10.1016/j.chemgeo.2012.07.032

Paris, G., Gaillardet, J., and Louvat, P., 2010, Geological evolution of seawater boron isotopic composition recorded in evaporites: Geology, v. 38, n. 11, p. 1035–1038, http://dx.doi.org/10.1130/G31321.1

Parkinson, I. J., Hammond, S. J., James, R. H., and Rogers, N. W., 2007, High-temperature lithium isotope fractionation: insights from lithium isotope diffusion in magmatic systems: Earth and Planetary Science Letters, v. 257, n. 3–4, p. 609–621, http://dx.doi.org/10.1016/j.epsl.2007.03.023

Pearce, C. R., Saldi, G. D., Schott, J., and Oelkers, E. H., 2012, Isotopic fractionation during congruent dissolution, precipitation and at equilibrium: Evidence from Mg isotopes: Geochimica et Cosmochimica Acta, v. 92, p. 170–183, http://dx.doi.org/10.1016/j.gca.2012.05.045

Pistiner, J. S., and Henderson, G. M., 2003, Lithium-isotope fractionation during continental weathering process: Earth and Planetary Science Letters, v. 214, n. 1–2, p. 327–339, http://dx.doi.org/10.1016/S0012-821X(03)00348-0

Pogge von Strandmann, P. A. E., Burton, K. W., James, R. H., van Calsteren, P., Gíslason, S. R., and Mokadem, F., 2006, Riverine behaviour of uranium and lithium isotopes in an actively glaciated basaltic terrain: Earth and Planetary Science Letters, v. 251, n. 1–2, p. 134–147, http://dx.doi.org/10.1016/j.epsl.2006.09.001

Pogge von Strandmann, P. A. E., Burton, K. W., James, R. H., van Calsteren, P., Gíslason, S. R., and Sigfússon, B., 2008, The influence of weathering processes on riverine magnesium isotopes in a basaltic terrain: Earth and Planetary Science Letters, v. 276, n. 1–2, p. 187–197, http://dx.doi.org/10.1016/j.epsl.2008.09.020

Pogge von Strandmann, P. A. E., Burton, K. W., James, R. H., van Calsteren, P., and Gíslason, S. R., 2010, Assessing the role of climate on uranium and lithium isotope behaviour in rivers draining a basaltic terrain: Chemical Geology, v. 270, n. 1–4, p. 227–239, http://dx.doi.org/10.1016/j.chemgeo.2009.12.002

Pogge von Strandmann, P. A. E., Elliot, T., Marschall, H. R., Coath, C., Lai, Y.-J., Jeffcoate, A. B., and Ionov, D. A., 2011, Variations of Li and Mg isotope ratios in bulk chondrites and mantle xenoliths: Geochimica et Cosmochimica Acta, v. 75, n. 18, p. 5247–5268, http://dx.doi.org/10.1016/j.gca.2011.06.026

Pogge von Strandmann, P. A. E., Opfergelt, S., Lai, Y.-J., Sigfússon, B., Gíslason, S. R., and Burton, K. W., 2012, Lithium, magnesium and silicon isotope behaviour accompanying weathering in a basaltic soil and pore water profile in Iceland: Earth and Planetary Science Letters, v. 339–340, p. 11–23, http://dx.doi.org/10.1016/j.epsl.2012.05.035

Poitrasson, F., Viers, J., Martin, F., and Braun, J.-J., 2008, Limited iron isotope variations in recent lateritic soils from Nsimi, Cameroon: implications for the global Fe geochemical cycles: Chemical Geology, v. 253, n. 1–2, p. 54–63, http://dx.doi.org/10.1016/j.chemgeo.2008.04.011

Richter, F. M., Davis, A. M., DePaolo, D. J., and Watson, E. B., 2003, Isotope fractionation by chemical diffusion between molten basalt and rhyolite: Geochimica et Cosmochimica Acta, v. 67, n. 20, p. 3905–3923, http://dx.doi.org/10.1016/S0016-7037(03)00174-1

Riebe, C. S., Kirchner, J. W., Granger, D. E., and Finkel, R. C., 2001, Strong tectonic and weak climatic control of long-term chemical weathering rates: Geology, v. 29, n. 6, p. 511–514, http://dx.doi.org/10.1130/0091-7613(2001)029⟨0511:STAWCC⟩2.0.CO;2

Riebe, C. S., Kirchner, J. W., and Finkel, R. C., 2004, Erosional and climatic effects on long-term chemical weathering rates in granitic landscapes spanning diverse climate regimes: Earth and Planetary Science Letters, v. 224, n. 3–4, p. 547–562, http://dx.doi.org/10.1016/j.epsl.2004.05.019

Rose, E. F., Chaussidon, M., and France-Lanord, C., 2000, Fractionation of boron isotopes during erosion processes: the example of Himalayan rivers: Geochimica et Cosmochimica Acta, v. 64, n. 3, p. 397–408, http://dx.doi.org/10.1016/S0016-7037(99)00117-9

Rudnick, R. L., Tomascak, P. B., Njo, H. B., and Gardner, R., 2004, Extreme lithium isotopic fractionation during continental weathering revealed in saprolites from South Carolina: Chemical Geology, v. 212, n. 1–2, p. 45–57, http://dx.doi.org/10.1016/j.chemgeo.2004.08.008

Ryu, J.-S., Jacobson, A. D., Holmden, C., Lundstrom, C., and Zhang, Z., 2011, The major ion, $\delta^{44/40}$Ca, $\delta^{44/42}$Ca, and $\delta^{26/24}$Mg geochemistry of granite weathering at pH = 1 and T = 25 °C: power-law processes and the relative reactivity of minerals: Geochimica et Cosmochimica Acta, v. 75, n. 20, p. 6004–6026, http://dx.doi.org/10.1016/j.gca.2011.07.025

Saulnier, S., Rollion-Bard, C., Vigier, N., and Chaussidon, M., 2012, Mg isotope fractionation during calcite precipitation: An experimental study: Geochimica et Cosmochimica Acta, v. 91, p. 75–91, http://dx.doi.org/10.1016/j.gca.2012.05.024

Savage, P. S., Georg, R. B., Williams, H. M., Turner, S., Halliday, A. N., and Chappell, B. W., 2012, The silicon isotope composition of granites: Geochimica et Cosmochimica Acta, v. 92, p. 184–202, http://dx.doi.org/10.1016/j.gca.2012.06.017

Schauble, E. A., Méheut, M., and Hill, P. S., 2009, Combining metal stable isotope fractionation theory with experiments: Elements, v. 5, n. 6, p. 369–374, http://dx.doi.org/10.2113/gselements.5.6.369

Schmitt, A.-D., Chabaux, F., and Stille, P., 2003, The calcium riverine and hydrothermal isotopic fluxes and the oceanic calcium mass balance: Earth and Planetary Science Letters, v. 213, n. 3–4, p. 503–518, http://dx.doi.org/10.1016/S0012-821X(03)00341-8

Schuessler, J. A., Schoenberg, R., and Sigmarsson, O., 2009, Iron and lithium isotope systematics of the Hekla volcano, Iceland—Evidence for Fe isotope fractionation during magma differentiation: Chemical Geology, v. 258, n. 1–2, p. 78–91, http://dx.doi.org/10.1016/j.chemgeo.2008.06.021

Sime, N. E., De La Rocha, C. L., Tipper, E. T., Tripati, A., Galy, A., and Bickle, M. J., 2007, Interpreting the Ca isotope record of marin biogenic carbonates: Geochimica et Cosmochimica Acta, v. 71, n. 16, p. 3979–3989, http://dx.doi.org/10.1016/j.gca.2007.06.009

Skulan, J. L., Beard, B. L., and Johnson, C. M., 2002, Kinetic and equilibrium Fe isotope between aqueous Fe(III) and hematite: Geochimica et Cosmochimica Acta, v. 66, n. 17, p. 2995–3015, http://dx.doi.org/10.1016/S0016-7037(02)00902-X

Spivack, A. J., Palmer, M. R., and Edmond, J. M., 1987, The sedimentary cycle of boron isotopes: Geochimica et Cosmochimica Acta, v. 51, n. 7, p. 1939–1949, http://dx.doi.org/10.1016/0016-7037(87)90183-9

Steinhoefel, G., Breuer, J., von Blanckenburg. F., Horn, I., Kaczorek, D., and Sommer, M., 2011, Micrometer silicon isotope diagnostics of soils by UV femtosecond laser ablation: Chemical Geology, v. 286, n. 3–4, p. 280–289, http://dx.doi.org/10.1016/j.chemgeo.2011.05.013

Teng, F.-Z., McDonough, W. F., Rudnick, R. L., Dalpé, C., Tomascak, P. B., Chappell, B. W., and Gao, S., 2004, Lithium isotopic composition and concentration of the upper continental crust: Geochimica et Cosmochimica Acta, v. 68, n. 20, p. 4167–4178, http://dx.doi.org/10.1016/j.gca.2004.03.031

Teng, F.-Z., Rudnick, R. L., McDonough, W. F., and Wu, F.-Y., 2009, Lithium isotopic systematics of A-type granites and their mafic enclaves: Further constraints on the Li isotopic composition of the continental crust: Chemical Geology, v. 262, n. 3–4, p. 370–379, http://dx.doi.org/10.1016/j.chemgeo.2009.02.009

Teng, F.-Z., Li, W.-Y., Rudnick, R. L., and Gardner, R., 2010, Contrasting lithium and magnesium isotope fractionation during continental weathering: Earth and Planetary Science Letters, v. 300, n. 1–2, p. 63–71, http://dx.doi.org/10.1016/j.epsl.2010.09.036

Thompson, A., Ruiz, J., Chadwick, O. A., Titus, M., and Chorover, J., 2007, Rayleigh fractionation of iron isotopes during pedogenesis along a climate sequence of Hawaiian basalt: Chemical Geology, v. 238, n. 1–2, p. 72–83, http://dx.doi.org/10.1016/j.chemgeo.2006.11.005

Tipper, E. T., Galy, A., and Bickle, M. J., 2006a, Riverine evidence for a fractionated reservoir of Ca and Mg on the continents: Implications for the oceanic Ca cycle: Earth and Planetary Science Letters, v. 247, n. 3–4, p. 267–279, http://dx.doi.org/10.1016/j.epsl.2006.04.033

Tipper, E. T., Galy, A., Gaillardet, J., Bickle, M. J., Elderfield, H., and Carder, E. A., 2006b, The magnesium isotope budget of the modern ocean: constraints from riverine magnesium isotope ratios: Earth and Planetary Science Letters, v. 250, n. 1–2, p. 241–253, http://dx.doi.org/10.1016/j.epsl.2006.07.037

Tipper, E. T., Galy, A., and Bickle, M. J., 2008a, Calcium and magnesium isotope systematics in rivers draining the Himalaya-Tibetan-Plateau region: lithological or fractionation control?: Geochimica et Cosmochimica Acta, v. 72, n. 4, p. 1057–1075, http://dx.doi.org/10.1016/j.gca.2007.11.029

Tipper, E. T., Louvat, P., Capmas, F., Galy, A., and Gaillardet, J., 2008b, Accuracy of stable Mg and Ca isotope data obtained by MC-ICP-MS using the standard addition method: Chemical Geology, v. 257, n. 1–2, p. 65–75, http://dx.doi.org/10.1016/j.chemgeo.2008.08.016

Tipper, E. T., Gaillardet, J., Louvat, P., Capmas, F., and White, A. F., 2010a, Mg isotope constraints on soil pore-fluid chemistry: evidence from Santa Cruz, California: Geochimica et Cosmochimica Acta, v. 74, n. 14, p. 3883–3896, http://dx.doi.org/10.1016/j.gca.2010.04.021

Tipper, E. T., Gaillardet, J., Galy, A., Louvat, P., Bickle, M., and Capmas, F., 2010b, Calcium isotope ratios in the world's largest rivers: A constraint on the maximum imbalance of oceanic calcium fluxes: Global Biogeochemical Cycles, v. 24, n. 3, GB3019, http://dx.doi.org/10.1029/2009GB003574

Tipper, E. T., Lemarchand, E., Hindshaw, R. S., Reynolds, B. C., and Bourdon, B., 2012a, Seasonal sensitivity of weathering processes: Hints from magnesium isotopes in a glacial stream: Chemical Geology, v. 312–313, p. 80–92, http://dx.doi.org/10.1016/j.chemgeo.2012.04.002

Tipper, E. T., Calmels, D., Gaillardet, J., Louvat, P., Capmas, F., and Dubacq, B., 2012b, Positive correlation between Li and Mg isotope ratios in the river waters of the Mackenzie Basin challenges the interpretation of apparent fractionation during weathering: Earth and Planetary Science Letters, v. 333–334, p. 35–45, http://dx.doi.org/10.1016/j.epsl.2012.04.023

Turner, B. F., Stallard, R. F., and Brantley, S. L., 2003, Investigation of in situ weathering of quartz diorite bedrock in the Rio Icacos basin, Experimental Forest, Puerto Rico: Chemical Geology, v. 202, n. 3–4, p. 313–341, http://dx.doi.org/10.1016/j.chemgeo.2003.05.001

Verney-Carron, A., Vigier, N., and Millot, R., 2011, Experimental determination of the role of diffusion on Li isotope fractionation during basaltic glass weathering: Geochimica et Cosmochimica Acta, v. 75, n, 12, p. 3452–3468, http://dx.doi.org/10.1016/j.gca.2011.03.019

Viers, J., Dupré, B., and Gaillardet, J., 2009, Chemical composition of suspended sediments in World Rivers: New insights from a new database: Science of The Total Enviroment, v. 407, n. 2, p. 853–868, http://dx.doi.org/10.1016/j.scitotenv.2008.09.053

Vigier, N., Decarreau, A., Millot, R., Carignan, J., Petit, S., and France-Lanord, C., 2008, Quantifying Li isotope fractionation during smectite formation and implications for the Li cycle: Geochimica et Cosmochimica Acta, v. 72, n. 3, p. 780–792, http://dx.doi.org/10.1016/j.gca.2007.11.011

von Blanckenburg, F., von Wirén, N., Guelke, M., Weiss, D. J., and Bullen, T. D., 2009, Fractionation of metal stable isotopes by higher plants: Elements, v. 5, n. 6, p. 375–380, http://dx.doi.org/10.2113/gselements.5.6.375

Welch, S. A., Beard, B. L., Johnson, C. M., and Braterman, P. S., 2003, Kinetic and equilibrium Fe isotope fractionation between aqueous Fe(II) and Fe(III): Geochimica et Cosmochimica Acta, v. 67, n. 22, p. 4231–4250, http://dx.doi.org/10.1016/S0016-7037(03)00266-7

West, A. J., Galy, A., and Bickle, M., 2005, Tectonic and climatic controls on silicate weathering: Earth and Planetary Science Letters, v. 235, n. 1–2, p. 211–228, http://dx.doi.org/10.1016/j.epsl.2005.03.020

White, A. F., Blum, A. E., Schulz, M. S., Vivit, D. V., Stonestrom, D. A., Larsen, M., Murphy, S. F., and Eberl, D., 1998, Chemical weathering in a tropical watershed, Luquillo Mountains, Puerto Rico: I. Long-term versus short-term weathering fluxes: Geochimica et Cosmochimica Acta, v. 62, n. 2, p. 209–226, http://dx.doi.org/10.1016/S0016-7037(97)00335-9

Wiederhold, J. G., Kraemer, S. M., Teutsch, N., Borer, P., Halliday, A. N., and Kretzschmar, R., 2006, Iron isotope fractionation during proton-promoted, ligand-controlled and reductive dissolution of goethite: Environmental Science and Technology, v. 40, n. 12, p. 3787–3793, http://dx.doi.org/10.1021/es052228y

Wiederhold, J. G., Teutsch, N., Kraemer, S. M., Halliday, A. N., and Kretzschmar, R., 2007a, Iron isotope fractionation in oxic soils by mineral weathering and podzolisation: Geochimica et Cosmochimica Acta, v. 71, n. 23, p. 5821–5833, http://dx.doi.org/10.1016/j.gca.2007.07.023

——— 2007b, Iron isotope fractionation during pedogenesis in redoximorphic soils: Soil Science Society of America Journal, v. 71, n. 6, p. 1840–1850, http://dx.doi.org/10.2136/sssaj2006.0379

Wiegand, B. A., Chadwick, O. A., Vitousek, P. M., and Wooden, J. L., 2005, Ca cycling and isotopic fluxes in forested ecosystems in Hawaii: Geophysical Research Letters, v. 32, n. 11, L11404, http://dx.doi.org/10.1029/2005GL022746

Wimpenny, J., James, R. H., Burton, K. W., Gannoun, A., Mokadem, F., and Gíslason, S. R., 2010a, Glacial effects on weathering processes: New insights from the elemental and lithium isotopic composition of West Greenland rivers: Earth and Planetary Science Letters, v. 290, n. 3–4, p. 427–437, http://dx.doi.org/10.1016/j.epsl.2009.12.042

Wimpenny, J., Gíslason, S. R., James, R. H., Gannoun, A., Pogge Von Strandmann, P. A. E., and Burton, K. W., 2010b, The behaviour of Li and Mg isotopes during primary phase dissolution and secondary mineral formation in basalt: Geochimica et Cosmochimica Acta, v. 74, n. 18, p. 5259–5279, http://dx.doi.org/10.1016/j.gca.2010.06.028

Wimpenny, J., Burton, K. W., James, R. H., Gannoun, A., Mokadem, F., and Gíslason, S. R., 2011, The behaviour of magnesium and its isotopes during glacial weathering in an ancient shield terrain in West Greenland: Earth and Planetary Science Letters, v. 304, n. 1–2, p. 260–269, http://dx.doi.org/10.1016/j.epsl.2011.02.008

Wischmeyer, A. G., De La Rocha, C. L., Maier-Reimer, E., and Wolf-Gladrow, D. A., 2003, Control mechanisms for the oceanic distribution of silicon isotopes: Global Biogeochemical Cycles, v. 17, n. 3, GB002022, http://dx.doi.org/10.1029/2002GB002022

Yesavage, T., Fantle, M. S., Vervoort, J., Mathur, R., Jin, L., Liermann, L. J., and Brantley, S. L., 2012, Fe cycling in the Shale Hills Critical Zone Observatory, Pennsylvania: An analysis of biogeochemical weathering and Fe isotope fractionation: Geochimica et Cosmochimica Acta, v. 99, p. 18–38, http://dx.doi.org/10.1016/j.gca.2012.09.029

Zhu, P., and McDougall, J. D., 1998, Calcium isotopes in the marine environment and the oceanic calcium

cycle: Geochimica et Cosmochimica Acta, v. 62, n. 10, p. 1691–1698, http://dx.doi.org/10.1016/S0016-7037(98)00110-0

Ziegler, K., Chadwick, O. A., White, A. F., and Brzezinski, M. A., 2005a, δ^{30}Si systematics in a granitic saprolite, Puerto Rico: Geology, v. 33, n. 10, p. 817–820, http://dx.doi.org/10.1130/G21707.1

Ziegler, K., Chadwick, O. A., Brzezinski, M. A., and Kelly, E. F., 2005b, Natural variations of δ^{30}Si ratios during progressive basalt weathering, Hawaiian Islands: Geochimica et Cosmochimica Acta, v. 69, n. 19, p. 4597–4610, http://dx.doi.org/10.1016/j.gca.2005.05.008